Effective anti-tumor immune responses are orchestrated by immune cell partnership network that functions through tissue homeostatic pathways, not direct cytotoxicity

Nicholas Koelsch[1,*], Faridoddin Mirshahi[2,3], Hussein F. Aqbi[4], Mulugeta Seneshaw[2,3], Michael O. Idowu[5,6], Amy L. Olex[6,7], Arun J. Sanyal[2,3,6], Masoud H. Manjili[1,6,8,*]

[1]Department of Microbiology & Immunology, Virginia Commonwealth University School of Medicine, Richmond, VA 23298, USA

[2]Department of Internal Medicine, VCU School of Medicine, Richmond, VA 23298, USA

[3]Stravitz-Sanyal Institute for Liver Disease and Metabolic Health, Richmond, VA 23298

[4]College of Science, Mustansiriyah University, Baghdad, P.O. Box 14022, Iraq

[5]Department of Pathology, VCU School of Medicine, Richmond, VA 23298, USA.

[6]VCU Massey Comprehensive Cancer Center, Richmond, VA 23298, USA

[7]C. Kenneth and Dianne Wright Center for Clinical and Translational Research, Virginia Commonwealth University School of Medicine

[8]VCU Institute of Molecular Medicine, Richmond VA 23298

[*]Corresponding Author: Masoud H. Manjili, Department of Microbiology & Immunology, VCU Massey Cancer Center, 401 College Street, Box 980035, Richmond, VA 23298, USA Phone: (804) 828-8779 email: masoud.manjili@vcuhealth.org; or Nicholas Koelsch, e-mail: koelschnj@vcu.edu

Keywords: systems immunology, hepatocellular carcinoma, nonalcoholic fatty liver disease, cancer dormancy, inflammation, network medicine, stromal cells

Abstract

The liver hosts a diverse array of immune cells that play pivotal roles in both maintaining tissue homeostasis and responding to disease. However, the precise contributions of these immune cells in the progression of nonalcoholic fatty liver disease (NAFLD) and hepatocellular carcinoma (HCC) remain unclear. Utilizing a systems immunology approach, we reveal that liver immune responses are governed by a dominant-subdominant hierarchy of ligand-receptor-mediated homeostatic pathways. In healthy individuals, inflammatory immune responses operate within these pathways, challenging the notion of the liver as a purely tolerogenic organ. Chronic consumption of a Western diet (WD) disrupts hepatocyte function and reconfigures immune interactions, resulting in hepatic stellate cells (HSCs), cancer cells, and NKT cells driving 80% of the immune activity during NAFLD. In HCC, 80% of immune response involves NKT cells and monocytes collaborating with hepatocytes and myofibroblasts to restore disrupted homeostasis. Interestingly, dietary correction during NAFLD yields nonlinear outcomes: tumor progression coincides with the failure of mounting homeostatic immune responses, whereas tumor prevention is associated with sustained immune responses, predominantly orchestrated by monocytes. These monocytes actively target fibroblasts and myofibroblasts, creating a tumor-suppressive microenvironment. Notably, only 5% of T cells displayed apoptosis-inducing activity, selectively contributing to the turnover of hepatic stromal cells, particularly myofibroblasts and fibroblasts. Our findings suggest that effective anti-tumor immune responses in the liver are primarily mediated by immune cells sustaining tissue homeostasis, rather than relying on direct cytotoxic mechanisms.

Introduction

Traditional interpretations of existing data suggest that immune responses are induced only in response to damage or infection, with the immune system being naturally tolerogenic to avoid reacting against harmless substances such as gut-derived nutrients in the liver (1). However, accumulating evidence challenges this view by demonstrating the presence of inflammatory immune responses under healthy conditions in the liver. The healthy liver maintains an active cytokine milieu, including pro-inflammatory cytokines such as IL-2, IL-7, IL-12, IL-15, TNF-α, and IFN-γ, as well as anti-inflammatory cytokines like IL-10, IL-13, and TGF-β, produced by the hepatic immune system (2). Additionally, activated NKT cells support hepatocyte proliferation and liver regeneration (3). Hepatic B and T cells also contribute to liver regeneration by producing lymphotoxin β (LTβ) (4), as the blocking of LTβR impedes liver regeneration after partial hepatectomy (5). Human hepatic $CD141^{+}$ dendritic cells (DCs) are potent cytokine producers and activators of T cells (6). This homeostatic inflammatory immune response is essential for hepatic cell regeneration and tissue remodeling. However, the mechanisms by which hepatic immune responses are induced under healthy conditions or nonalcoholic fatty liver disease (NAFLD) and hepatocellular carcinoma (HCC) remain elusive. The present study addresses this gap by the assessment of the hepatic immune system under healthy condition on a regular chow diet (CD) as well as during the progression or inhibition of HCC.

The immune system in each organ, including the liver, operates through a complex network of reciprocal cis and trans cellular interactions via ligand-receptor communications. Understanding this system requires a holistic perspective rather than focusing on individual cell types alone. This systems perspective is crucial for both the immunobiology of diseases and the development of novel immunotherapies. While reductionist approaches in immunology have advanced our

knowledge of immune cell types, they fall short in uncovering the mechanisms of emergent collective functions of the organ-specific immune system, and in offering curative immunotherapies beyond prolonging the survival of cancer patients. Recent reviews have highlighted contradictory observations regarding the dual functions of innate and adaptive immune responses in tumor immune surveillance, inflammation-associated liver protection or liver damage, and promotion or inhibition of HCC (7,8).

Recent advancements in big data and computational algorithms have enabled the detection of cellular interactions as distinct networks, providing deeper insights into disease mechanisms. By adopting a systems immunology approach for understanding the progression of NAFLD to HCC, it has been demonstrated that dominant-subdominant relationships among hepatic immune cells shape immunological patterns from which collective functions emerge, distinct from the individual roles of each immune cell type (9,10). These dominant-subdominant interactions are analogous to "cell competition" or "cellular fitness," where winner cells survive and eliminate loser cells (11,12). In the present study, we focused on the molecular pathways of ligand-receptor interactions to uncover immunological patterns associated with dominant cell types and pathways involved in the progression or inhibition of HCC in the DIAMOND mouse model. This approach allows for a more comprehensive understanding of the mechanisms of NAFLD and HCC, as well as the development of more effective therapeutic strategies. Such interactions network analysis of hepatic cells revealed the presence of carcinogenic processes prior to the formation of HCC on a WD, as well as during rescue from HCC through dietary correction, indicating the presence of dormant cancer. Additionally, cellular partnership that promoted liver homeostatic pathways was found to be a crucial mechanism of hepatic immune surveillance for preventing HCC.

Materials and Methods

Animal model and experimental design

Diet-induced animal model of nonalcoholic fatty liver disease (DIAMOND) (13) were used in this study, which are an isogenic cross between C57BL/6J and 129S1/SvImJ mice. In brief, male mice were put on a standard CD for 40 weeks (n=2), WD, or underwent diet reversal (RD) after being on a WD. A WD consists of high fructose and glucose sugar water in conjunction with high-fat diet (10). Only male mice were used in this study due to higher incidence of males developing HCC than female mice on a WD (10). Mice were on a WD for 40 weeks prior to the development of HCC and during NAFLD (the WD.nf group; n=2) or after development of HCC by 48 weeks (WD.t; n=3). Separate groups underwent diet reversal for additional 12 weeks, after 36 weeks of being on a WD, in which some mice developed tumors (RD.t; n=2) and some were rescued from the development of HCC and exhibited no tumors in the livers (RD.n; n=3) (Figure S1).

Hematoxylin and eosin staining

Formalin fixed paraffin embedded liver (FFPE) tissues were subjected to hematoxylin and eosin (H & E) stain using Tissue Tek Prisma Autostainer as previously described by our group (14). Histology slides were scanned at 40x magnification.

Flow cytometry

Multicolor staining and flow cytometry analysis of T cells were performed as previously described by our group (10). Briefly, Fc blocker anti-CD16/32 Ab was used for all staining panels before using the T cell staining panel (CD8, CD4, CD44, CD62L). All reagents were

purchased from Biolegend (San Diego, CA). All reagents were used at the manufacturer's recommended concentration. Multicolor data acquisition was performed using a LSRFortessa X-20 (BD Biosciences) and a ImageStreamX Mark II Imaging Flow Cytometer (Millipore Sigma, Billaerica, MA). Data were analyzed using FCS Express v5.0 (De Novo Software; Glendale, CA). The FVS negative viable cells were gated on CD4+ or CD8+ T cells, and analyzed for $CD44^{+}CD62L^{-//low}$ T effector (Te), $CD44^{+}CD62L^{+/high}$ (Tcm) and $CD44^{-}CD62L^{+}$ T naïve (Tn) subsets.

Quality control and filtering

Single nuclei RNA-seq data from all samples was provided by the Novogene company, in which nuclei were isolated from frozen mouse liver and tumor samples, and using 3' single cell gene expression libraries. Novogene performed unique molecular identifier (UMI) collapsing, alignment to mouse reference genome mm10-5.0.0, and UMI counting and initial quality control. Additionally, Novogene used Cell Ranger version 7.0.0 and introns were included in the analysis. Seurat version 4.4.0 (15) was used to handle all data and perform quality control and filtering metrics. In brief, samples were loaded into the VCU HPRC core clusters to mark data with group identifying labels (CD, WD.nf, WD.t, RD.t, RD.n), and filter cells with nFeature_RNA > 200 and < 5000, as well as for cells expressing < 5% mitochondrial associated genes. The threshold for nFeatureRNA > 200 and < 5000 is to ensure there are sufficient molecular transcripts in one cell and 5000 > may entail two cells in one run, whereas mitochondrial gene percentages higher than 5% may be indicative of dead/dying cells. High Performance Computing resources provided by the High Performance Research Computing (HPRC) core facility at Virginia Commonwealth University (https://hprc.vcu.edu) were used for conducting the research reported in this work.

Cell type annotation and quantification

Markers for major liver cell types specific for mice from liver focused data were extracted from the CellMarker 2.0 database (16) and compiled into one comprehensive list to annotate cells. The scSorter R program version 0.0.2 (17) was used in conjunction with these marker genes to annotate liver immune and nonimmune cell types such as B cell, T cell, DC, NKT, NK, neutrophil, monocyte, macrophage, endothelial, LSEC, stromal, HSC, fibroblast, myofibroblast, cholangiocyte, hepatocyte, and cancer cells. Following annotation, the cells were clustered and visualized in Seurat with UMAP after removing any cells classified as "Unknown" for subsequent analyses. Cellular annotations were confirmed by making heatmaps of marker genes specific for each cell type of interest. Further, quantification of the exact number of cells was performed in excel and normalized to 100% to show the composition of cell types in each group in the study, such as immune cells and nonimmune cells. Violin plots of specific marker genes in various cell type populations across groups were visualized and quantified in Seurat with the VlnPlot function. Assessments of specific genes such as Mki67 (Ki67), Tnfsf10 (TRAIL)/Tnfrsf10b (TRAILR2), FasL/Fas were performed in Seurat with the DotPlot function, and average transcript expression was quantified with AverageExpression function after filtering cell populations for only cells expressing the gene of interest (>0).

Intercellular communication networks

CellChat version 2.1.1 (https://doi.org/10.1101/2023.11.05.565674) was utilized with default parameters (trimean approach requiring 25% of the cells in a population to express a specific ligand or receptor to be considered for statistical testing) to evaluate ligand and receptor (L-R) interactions amongst all annotated cell types. First, we performed this on all groups, and subsequently performed the same analysis with a "truncated mean" of 0.05 with the

computeCommunProb function to evaluate lowly expressed immunologically relevant interactions in 5% of cells within each annotated cell type, as well as with a “truncated mean” of 0.75 to assess major communication networks in 75% of cells, however the capacity of filtering can only evaluate those in 50% of cells through the use of “truncated mean” of 0.50, as results from 0.75 were identical to 0.5. Additionally, by filtering L-R detection through the identifyOverExpressedGene function and filtering thresh.pc = 0.80 allows analysis of only L-R pairs expressed in 80% of each cell population. Comparative CellChat analyses were also employed to address any changes in each cell type across groups, in which the sum of probability scores for cell types of interest were also quantified in excel to highlight the incoming and outgoing interaction strength in experimental groups. Analysis of differential number of interactions was performed to visualize the number of L-R interactions sent from one cell type to all others detected in one condition compared to the first, seen by red arrows indicating increased signaling events and blue arrows indicating decreased signaling events. Signaling pathway changes were analyzed similarly to compare major pathways utilized by a specific cell type in one condition compared to the first. Versions of additional dependencies for CellChat data visualization include NMF version 0.27 (https://github.com/renozao/NMF), circlize version 0.4.16 (https://github.com/jokergoo/circlize), and ComplexHeatmap version 2.20.0 (https://github.com/jokergoo/ComplexHeatmap).

Statistical analysis

CellChat identifies differentially expressed signaling genes via Wilcoxon rank sum test filtering for those at a 0.05 significance level, followed by averaging gene expression across a given cell group, generation of intercellular communication probability values for each L-R interaction, and finally identifying statistically significant communications through permutation tests and

recalculating communication probability between cell groups (18). Chord diagrams of signaling directionality were further filtered to only include L-R signaling interactions that were at or below a p-value of 0.01. Quantification of gene expression levels, such as Hnf4α and Ki67, were averaged across replicates and calculated standard error mean by the standard deviation of expression levels in sample replicates divided by the square root of the number of sample replicates.

Data and code availability

All code and gene lists for sorting cells are available on GitHub (https://github.com/koelschnj/Systems-Approaches-Understanding-Liver-Cell-Networks-NAFLD-HCC-DietReversal) and is publicly available on the following links through the Gene Expression Omnibus (GEO) (18) : https://www.ncbi.nlm.nih.gov/geo/query/acc.cgi?acc=GSE225381 and https://www.ncbi.nlm.nih.gov/geo/query/acc.cgi?acc=GSE279124. The CD and WD.nf datasets analyzed during the current study are available in the GEO repository, GSE225381. The WD.t, RD.t, and RD.n datasets generated and analyzed during the current study are available in the GEO repository, GSE279124.

Materials availability

DIAMOND mice used in this study will be provided, upon request to the lead contact, and may require fulfillment of an MTA. This study did not generate new unique reagents.

Results

Carcinogenic events take place during NAFLD and remain dormant during rescue from HCC

The livers of male DIAMOND mice that were on a CD or WD or reversal of a WD to a CD for 12 weeks starting from 36 weeks of being on a WD were examined and subjected to hematoxylin-eosin (H&E) staining and single nuclei RNA sequencing (snRNAseq) analysis when animals reached 13 months of age (Figure S1). There was no macroscopic or microscopic tumor detectable in the liver of animals during NAFLD at 11 months of age (WD.nf) or rescue from HCC following diet correction at 13 months of age (RD.n) (Figure 1A). However, cell annotation and UMAP clustering of nonimmune cells revealed a cancer fraction in the liver (Figure 1B), characterized by the oncogenic glypican-3 (GPC3) and alpha-fetoprotein (AFP), as well as the tumor suppressor retinoblastoma 1 (Rb1) and hepatocyte nuclear factor 4 alpha (HNF4α), separating them from hepatocytes (Figure 1C). Further filtration of the cancer fractions based on the expression of GPC3 oncogene transcript, which is more sensitive than AFP in the diagnosis of liver cancer (19), revealed the expression of all tumor markers in the WD.t group and two markers in the CD group (Figure 1D). Among these groups, high level of HNF4α transcript in the RD.n group (Figure 1E) was associated with rescue from HCC, whereas low level of HNF4α transcript in the WD.nf and RD.t groups (Figure 1E) was associated with NAFLD and HCC, respectively. In the CD group, the tumor suppressor HNF4α (20) was at the highest levels compared to other groups (Figure 1E). Although the presence of cancer cells in CD was minimal (Figure 1B), this may be due to age-associated carcinogenesis events. Further analysis of the CD, WD.nf and RD.n groups showed differential average transcript for Ki67 expression between the tumor and hepatocyte fractions. While hepatocytes showed high level of Ki67 transcripts (>5) in the WD.nf group compared to intermediate levels (between 2-5) in the CD and RD.n groups, tumor fractions showed Ki67 negative quiescent cells in the CD group and $Ki67^{low}$ (<2) indolent cells in the WD.nf and RD.n groups (Figure 1F). We have already reported

that indolent dormant cells establish cancer as opposed to quiescent cells remaining dormant (21,22). It is yet to be determined whether such malignant events signify tumor dormancy or the presence of cancer stem cells. We have previously detected such tumor dormancy in the FVBN202 transgenic mouse model of breast cancer (21).

Hepatic immune responses are induced by hepatic structural cells for participating in liver homeostasis pathways during healthy condition

We aimed to investigate the crosstalk between hepatic structural cells and immune cells during liver tissue homeostasis under normal physiological conditions. To achieve this, we analyzed the livers of one-year-old mice that had been on a regular CD for 40 weeks, using scSorter and CellChat Analyses. Immune cells were quantitatively dominated by B cells, T cells and macrophages (Figure 2A). However, the receptor-ligand interaction analyses revealed dominance of hepatocytes accounting for 80% of them sending homeostatic PARs signal to themselves, cholangiocytes, HSCs and stromal cells (Figure 2B). Among immune cells, macrophages and monocytes dominated the ligand-receptor network such that 50% of macrophages collaborated with hepatocytes in homeostasis of HSCs and myofibroblasts via IGF signaling, and 50% of monocytes collaborated with hepatocytes, fibroblasts and HSCs for the adhesion, function and remodeling of hepatocytes through the FN1-SDC4 pathway (23) (Figure 2C). The IGF-IGFR1 pathway is involved in normal glucose homeostasis in the liver (24), the activation of myofibroblasts and HSCs, as well as modulation of DC maturation (25). Also, 50% and 25% of macrophages received GAS signaling from cholangiocytes and myofibroblasts, respectively (Figure 2C-D). GAS signaling can promote efferocytosis of macrophages (26,27). The homeostatic pathways utilized by 25% of all immune cells included FN1 that supported immune cells activation and liver tissue integrity and cell-matrix remodeling, as well as VTN that

targeted HSCs and macrophages for cell-matrix remodeling and phagocytosis of macrophages (Figure 2D). Around 25% of hepatocytes and cholangiocytes were involved in the activation of immune cells through Galectin 9 and Spp1, respectively (Figure 2D). Galectin 9 has been reported to induce T cell activation through the engagement with the dominant pathway CD45 that regulates signaling thresholds by dephosphorylating components of the Src kinase family, and LcK-dependent calcium mobilization in peripheral $CD4^+$ T cells (28). Also, the Galectin 9-CD44 interaction enhances stability and function of adaptive Tregs (29). Finally, Galectin 9 binds IgM-BCR to regulate B cell signaling (30). Hepatic structural cells participated in the activation of innate immune cells using laminin and collagen homeostatic pathways (Figure 2D). Targeting Dag1 in laminin pathway can activate phospholipase C gamma (PLC-γ) downstream of the TcR-CD1d in NKT cells (31). Finally, immune cells and structural cells participated in the modulation of the immune responses through the anti-inflammatory DHEAS that targeted PPARα (32,33) (Figure 2D). Analysis of the nuclear transcription factors associated with immune cell activation showed presence of activated T cells (NFAT), NKT and NK cells (T-bet and Id2), macrophages (pro-inflammatory C/EBPβ and anti-inflammatory PPARγ), and monocytes (SPI1/PU.1) (Figure 2E). Along this line, flow cytometry analysis of the hepatic T cells showed presence of $CD44^+/CD62L^{-/low}$ $CD4^+$ Te and $CD8^+$ Te cells in the liver (Figure S2A). Consistent with our observations, it was reported that both $CD4^+$ and $CD8^+$ T cells, but not γδ T cells, are required for normal liver regeneration through lymphotoxin production such that $RAG1^{-/-}$ mice show extensive hepatic injury following partial hepatectomy (34). These data suggest the tissue-based direct activation of the immune cells as well as participation of activated immune cells in liver homeostasis during normal condition.

Regarding immune cell cytotoxicity, only 5% of NK cells and NKT cells were involved in TRAIL-mediated turnover of fibroblasts. Additionally, 5% of NK cells and T cells were involved in Fas-L-mediated turnover of fibroblasts, endothelial cells, LSEC, myofibroblasts, and hepatocytes (Figure S2B). All these hepatic structural cells were found to express MHC class I molecules, primarily H2-Q10 and H2-K1 (Figure S2C).

HCC progression or inhibition is driven by hepatic cellular interaction network modulating liver microenvironment through NKT cell and monocyte-dominated immune responses

The hepatic cells were analyzed for the identification of cell types of which 50% participated in ligand-receptor interactions network. The highest number and strength of ligand-receptor interactions were evident during WD as well as rescue from HCC following diet reversal (Figure 3A). These data suggest that such cell-cell communication network may be of host-protective nature such that its maintenance was associated with the rescue of animals from HCC following dietary correction. In order to identify cell types that dominate the communication networks under each condition, cell type ratios and cell-cell interactions were analyzed. In all groups, hepatocytes and macrophages were dominant cell populations compared to other nonimmune and immune cell types (Figure 3B, left panels). However, the ligand-receptor interactions showed dominant NKT cells during NAFLD with monocytes joining them during HCC on a WD. Maintenance of monocytes dominance during diet reversal was associated with rescue from HCC (Figure 3B, left panels). Although there are contradictory reports on the role of NKT cells as well as T cells, macrophages, and monocytes in promoting or inhibiting HCC (35–42), our data suggest that NKT cell signaling network became dominant in response to WD, as they disappeared following diet correction. Also, monocytes were active in sending signals for

protecting from HCC in the WD.t group, but they did not succeed because of chronic intake of a WD; however, their signaling retention during diet correction rescued animals from HCC, whereas disappearance of their signaling network resulted in HCC progression following dietary correction.

Among nonimmune cell communications network, cancer cells were dominant during NAFLD or HCC following dietary correction, with myofibroblasts, hepatocytes and fibroblasts joining them during HCC on a WD or rescue from HCC (Figure 3B, right panels). These data suggest that cancer cells, both as dormant and proliferating tumor, dominate the ligand-receptor interactions network.

NKT cells and cancer cells dominate cellular interaction network with NKT cells orchestrating the hepatic immune responses mainly through homeostatic pathways, rather than cytotoxic pathways, during WD-induced NAFLD progression

We have previously reported that collective function of the hepatic structural cells or immune cells is determined by dominant-subdominant interactions within the cellular networks (9,10,43). Here, we sought to determine molecular pathways that dominate cell-cell interactions during the progression of NAFLD. Although pattern of cellular distribution showed dominant hepatocytes and macrophages (Figure 4A), analysis of signaling pathways revealed NKT cells and cancer cells dominating 80% of the ligand-receptor cellular interactions (Figure 4B). This included sending homeostatic cholesterol and PARs signaling to themselves and other hepatic structural cells, excluding hepatocytes, as well as activating all immune cells, except NKT cells, through the LcK activating Galectin 9-CD45 pathway or activating monocytes through the FN1 interacting with the co-stimulatory VLA-4 (Itga4+Itgb1) (44) (Figure 4B). Such dominant NKT cell response was associated with the expression of CD1d on hepatic cells, particularly on cancer

cells (Figure 4C). Cholesterol targeting RoRα induces fatty acid oxidation and modulation of inflammation in immune cells (45) during immune responses (46) as well as affecting liver structural cells for hepatic lipid homeostasis (47). PARs signaling facilitates cell polarity and tight junctions which are essential for maintaining the integrity of the liver tissue, and facilitating hepatocytes repair and regeneration process during liver injury, though 80% of hepatocytes lost this homeostatic pathway while cancer cells received PARs signaling during NAFLD (Figure 4B). Analysis of 50% of cells contributing to the ligand-receptor interaction network showed similar pattern with a broader receptor targeting of the structural cells and immune cells (Figure 4D). Cancer cells and NKT cells participated in the activation of all immune cells through Galectin 9-CD45/CD44 pathway, with cholangiocytes and HSCs joining them in activating macrophages and monocytes through FN1-CD44/VLA-4 pathway (Figure 4D). Other homeostatic signaling pathways contributing to the activation of macrophages, monocytes and NKT cells included laminin and collagen signaling pathways, as well as NKT cells participating in homeostasis of endothelial cells and LSEC via VEGF (Figure S3).

Since signaling network dominance by hepatocytes during CD shifted to NKT cell and cancer cell signaling dominance during NAFLD, we performed a comparative analysis of signaling directionality between these groups. During NAFLD, the interaction networks accounting for 50% of cells were dominated by cancer, HSCs and NKT cells (Figure 4E). The majority of signaling communication was also observed between these three dominant cellular networks, with NKT cells also sending higher number of signals to myofibroblasts than to HSCs (Figure 4F). In cancer cells and NKT cells, the significantly increased signals included reciprocal PARs, cholesterol, Galectin 9 and FN1, while in HSCs they included receiving cholesterol and sending FN1 signals (Figure 4G). Although 50% of other immune cells were not involved in sending

these homeostatic signals, they were impacted by these signals mainly from NKT cells and cancer cells (Figure S4A). Among 50% of other hepatic structural cells, all but hepatocytes and fibroblasts were impacted mainly by NKT cells and cancer cells, and sent signals to NKT cells and macrophages (Figure S4B).

TRAIL-mediated cytotoxic immune responses were detected in 5% of NK cells and T cells targeting fibroblasts that expressed highest level of TRAILR2 (Figure S5A, left panels). Fas-mediated cytotoxic immune responses were also detected in 5% of NK cells and T cells targeting hepatic structural cells, mainly cancer, myofibroblasts and endothelial cells (Figure S5A, right panels). The hepatic target cells expressed MHC class I (Figure S5B).

The hepatic cellular interaction network dominated by cancer cells, hepatocytes, and myofibroblasts induce NKT cell and monocyte-dominated immune responses mainly through liver homeostatic pathways during HCC on a WD

While hepatocytes and macrophages remained dominant cells during HCC on a WD (Figure 5A), 80% of the ligand-receptor interaction network was dominated by NKT cells and monocytes as well as cancer, hepatocytes and myofibroblasts, which communicated via six homeostatic signals (Figure 5B). Among these signals, PARs and FN1 were sent by all immune cells to hepatic structural cells, cancer cells, NKT cells, and monocytes, while DHEAS, 27HC, and FGF were sent by NKT cells and monocytes to themselves, hepatic structural cells, and cancer cells (Figure 5B). NKT cells and monocytes also delivered VEGF to endothelial cells and LSEC (Figure 5B). In immune cells, PARs signaling promotes phagocytosis in macrophages and monocytes by facilitating the formation of the phagocytic cup, and also supports the formation of the immune synapse, enabling efficient cell-cell communication and T cell activation. The FN1-SDC4 pathway induces myofibroblasts and fibroblasts to promote tissue healing as well as

proinflammatory cytokine secretion by NKT cells and monocytes, while DHEAS, 27HC, and FGF regulate their inflammatory functions. These dominant signaling pathways engaged additional receptors, such as Itgav-Itgb1, CD44, PPARγ, and FGFR4, accounting for 50% of cell-cell interactions (Figure 5C).

In order to determine signaling pathways induced in the presence of HCC, comparative analyses between the WD.t vs. WD.nf groups were performed on 50% threshold analysis. Among these dominant nonimmune cells, hepatocytes and fibroblasts dominantly communicated with NKT cells, whereas cancer and myofibroblasts communicated with monocytes during HCC (Figure 5D). All these dominant cells upregulated CD1d during HCC (Figure S6), which could present glycolipid to NKT cells for their activation. All other hepatic structural cells communicated mainly with monocytes or NKT cells (Figure S7A). Specifically, stromal cells that did not show active communications during NAFLD (Figure 4), dominated their communications with NKT cells during HCC on a WD (Figure S7A).

Among immune cells, NKT cells showed the highest number of signals towards fibroblasts and hepatocytes while monocytes mainly targeted cancer cells, though both of them were mainly impacted by each other, hepatocytes, myofibroblasts and fibroblasts (Figure 5E). All other immune cells sent highest number of signals to NKT cells, but they received highest number of signals from monocytes, myofibroblasts or fibroblasts (Figure S7B). Compared to NAFLD, the HCC group showed new homeostatic signaling (PARs, FN1, DHEAS, 27HC and FGF) in monocytes, hepatocytes, myofibroblasts and fibroblasts, while these signals were also active in NKT cells during NAFLD but they were upregulated during HCC (Figure 5F). TRAIL- and Fas-mediated cytotoxicity were detected in 5% of T cells, primarily targeting fibroblasts expressing TRAILR2, as well as cancer cells, fibroblasts, and endothelial cells expressing Fas (Figure S8A-

B). All the target cells expressed MHC class I (Figure S8C). Such homeostatic pathways were induced to protect the liver from a toxic WD, but their chronic activation due to continuous consumption of a WD led to fibrinogenesis and HCC.

Stromal cell and cancer cell-dominated interaction network and failure to maintain homeostatic immune responses promote HCC whereas myofibroblast, fibroblast and monocyte-dominated interaction network involving homeostatic pathways prevent HCC following dietary correction

In order to determine whether correction of diet during NAFLD can rescue animals from HCC and restore immune cell interaction network similar to that in the CD control group, animals were switched to a CD after 36 weeks of being on a WD. While hepatocytes, cancer and macrophages dominated cellular pattern during tumor progression, monocytes and neutrophils emerged as dominant cells during rescue from HCC (Figure 6A). However, analysis of the ligand-receptor interactions representing 80% of cells showed a functional dominance of cancer, stromal cells, cholangiocytes and DCs in sending PARs signaling to themselves but not to hepatocytes during tumor progression (Figure 6B, left panels). On the other hand, rescue from HCC was associated with the functional dominance of monocytes, myofibroblasts and fibroblasts in sending the homeostatic signals PARs, DHEAS, NRG and PROS to themselves and to macrophages, hepatocytes and cancer cells (Figure 6B, right panels). Also, all immune cells participated in PARs signaling pathway. For 50% of cells, stromal cells and cancer cells dominated cellular interaction network involving PARs, DHEAS, PROS, FN1 and VTN which modulated monocytes and DCs during tumor progression (Figure 6C, left panels). However, rescue from HCC was associated with the dominance of monocytes, myofibroblasts and fibroblasts with the addition of cholesterol and FGF signaling pathways (Figure 6C, right

panels). Monocytes also began to produce DHEAS that shifted towards targeting hepatocytes, fibroblasts and myofibroblasts during rescue from HCC (Figure 6C). PROS produced by monocytes shifted from targeting DCs and stromal cells towards targeting macrophages and myofibroblasts during rescue from HCC (Figure 6C). Also, FN1 produced by more innate immune cells with shifts toward targeting hepatocytes, fibroblasts and myofibroblasts during rescue from HCC (Figure 6C). VTN also produced by all immune cells and shifted from targeting monocytes to targeting myofibroblasts during rescue from HCC (Figure 6C).

In order to determine whether rescue from HCC following dietary correction was associated with the restoration of the signaling network as in the healthy CD group, comparative analysis of dominant cellular interaction signaling was performed on the 50% threshold setting. Among dominant functional cells during tumor progression, stromal cells and cancer cells showed significantly increased communications with themselves and with monocytes, while they targeted mainly myofibroblasts or fibroblasts during rescue from HCC (Figure 6D). Among dominant functional cells during rescue from HCC, myofibroblasts and fibroblasts showed significantly increased communications with themselves as well as with monocytes, hepatocytes and cancer cells only during rescue from HCC but not during HCC progression (Figure 6D). Finally, monocytes being dominant during both HCC progression and inhibition, showed significantly increased number of homeostatic signaling communications towards all immune cells and hepatic structural cells, myofibroblasts and fibroblasts in particular, only during rescue from HCC (Figure 6D). These homeostatic signaling pathways included new communication signals that were not present in the CD group, of which FGF and cholesterol were found to be specific to the RD.n group during rescue from HCC (Figure 7A-B). In addition, FGF, HGF, cholesterol and NRG were found to be specific to the RD.n group during rescue from HCC

(Figure 7A-B). Myofibroblasts showed a new VTN signal sent to monocytes during HCC whereas they sent numerous new signals (FN1, PARs, DHEAS, PROS, galectin, 27HC, cholesterol, ANGPTL, NRG, Spp1, testosterone and CypA) to hepatic structural cells during rescue from HCC (Figure 7A-B). Similar pattern of new cellular signaling pathways were detected in fibroblasts and hepatocytes (Figure 7A-B). Finally, monocytes sent several new signaling pathways following diet reversal compared to those during CD, of which PARs, DHEAS, 27HC, Cholesterol and NRG were found to be new signals specifically increased during rescue from HCC (Figure 7A-B). Other hepatic cells and immune cells followed similar pattern of cellular signaling directionality (Figure S9A-B).

TRAIL-mediated cytotoxicity was below a 5% threshold, whereas Fas-mediated cytotoxicity was detected in 5% of T cells in both groups (Figure S10A-B). This cytotoxicity primarily targeted cancer cells, stromal cells, and endothelial cells during tumor progression, while during the rescue from HCC, it targeted myofibroblasts, fibroblasts, endothelial cells, and LSEC (Figure S10A-B). All the target cells expressed MHC class I (Figure S10C).

Discussion:

Under the influence of toxins due to chronic consumption of a high-fat and high-sugar WD, the liver experiences a range of metabolic stresses and inflammatory signals that can initiate early carcinogenic processes, which may remain dormant until the development of HCC (48). We have previously reported the existence of cancer cell dormancy in the FVBN202 transgenic mouse model of spontaneous breast cancer (21), as well as hepatic carcinogenesis events in the DIAMOND model of NAFLD progression to HCC (9). In this study, we employed a systems immunology approach to investigate how immune cells interact within complex cellular networks to coordinate hepatic immune responses. Our findings reveal that carcinogenic events

occur during the progression of NAFLD, preceding the onset of HCC, with tumors remaining dormant during the rescue from HCC. Notably, these dormant cancer cells actively participated in a cell-cell communication network with hepatic structural cells and immune cells.

Our findings indicate that the liver is not a tolerogenic organ under healthy conditions. Instead, it utilizes hepatic homeostatic pathways to activate immune cells, whose primary role is to support liver homeostasis. The effector functions of hepatic immune cells are mediated through a ligand-receptor interaction network that is influenced more by the targeted cells than by the functions of the effector immune cells alone. In this context, macrophages and monocytes play a dominant role, comprising 50% of the cellular population, compared to other immune cells, which account for 25%. Notably, only 5% of T cells, NKT cells, or NK cells exhibited TRAIL- or Fas-mediated cytotoxic functions, primarily participating in the homeostatic turnover of hepatic structural cells, mainly fibroblasts, endothelial cells, and LSEC. This tissue-based activation of the immune response is further evidenced by the presence of tissue-resident T memory cells (Trm). Additionally, the primary function of immune responses has been proposed to be participation in the homeostasis of their target cells (49). This homeostatic function can explain the observation that auto-reactive T cells are unable to induce autoimmune pancreatitis following the adoptive transfer of OVA-specific T cells, which recognize and become activated by OVA-expressing pancreatic cells (50).

Such homeostatic immune responses are elevated during NAFLD and HCC to support liver cell integrity, which is disrupted by a WD. NKT cells and dormant tumor cells play a dominant role in the cellular interaction network through cholesterol and PARs signaling to liver cells, as well as Galectin 9 and FN1 signaling to immune cells. This interaction activates immune cells via CD45 and the co-stimulatory receptor VLA-4. During HCC, similar pathways involved in tissue-

induced immune responses, as well as hepatic homeostatic pathways, are engaged, with monocytes joining NKT cells as the dominant immune cells. These homeostatic immune responses are robustly activated to protect the liver from the toxicity of a WD; however, their chronic activation due to continuous WD consumption leads to fibrogenesis and HCC. This observation is consistent with other reports indicating that hepatic $CXCR6^+$ NKT cells inhibit the progression of NAFLD to HCC in C57BL/6J mice (51). Notably, the hepato-protective role of NKT cells is more pronounced in male compared to female mice models of NAFLD (35). Additionally, the host-protective role of NKT cells has been documented in mouse models induced by fast food diet (FFD) and methionine-choline-deficient (MCD) diet; however, chronic administration of α-GalCer can induce NKT cell anergy and promote disease progression (36), suggesting that NKT cells may become overwhelmed by chronic WD intake.

These data suggest that the inflammatory immune responses observed during NAFLD and HCC are inherently host-protective. However, chronic exposure to carcinogenic factors can overwhelm hepatic immune responses, hindering injury healing and leading to chronic inflammation that exacerbates liver damage. Furthermore, the traditional view that pro-inflammatory M1 macrophages are anti-tumor and anti-inflammatory M2 macrophages are pro-tumor may be a misunderstanding of the hepatic immune responses, which function flexibly to protect the host by mediating inflammatory immune responses while simultaneously preventing further damage by inhibiting chronic inflammation. Therefore, inducing a transition from M2 to M1 macrophages may not be the most effective strategy, as this approach has failed to treat HCC. Instead, it is essential to identify and control the carcinogenic pressures to enable endogenous immune responses to manage cancer. To test this hypothesis, we eliminated carcinogenic WD consumption during NAFLD by switching from a WD to a control CD. We

observed that sustained immune responses through hepatic homeostatic pathways, which were present during HCC on a WD, prevented the development of HCC following dietary correction. In contrast, failure to maintain these immune responses resulted in HCC progression even after dietary correction.

These findings indicate that homeostatic inflammatory immune responses during NAFLD and HCC on a WD are host-protective; removal of toxic pressures allows the immune response to promote hepatic tissue healing and prevent HCC. Our results align with recent reports on Resmetirom, which treats patients with metabolic dysfunction-associated steatohepatitis (MASH) by restoring liver homeostasis (52). Additionally, homeostatic immune responses targeting all hepatic cells, particularly myofibroblasts and fibroblasts, proved to be more protective against HCC than those focused solely on cancer or stromal cells. Myofibroblasts are significant contributors to the remodeling of the extracellular matrix (ECM) for liver repair. While chronic activation of myofibroblasts can lead to fibrinogenesis, they also hinder tumor growth by mechanically restricting tumor spread through type I collagen production and expressing the cytoprotective molecule cytoglobin (Cygb) which reduces oxidative stress. Moreover, they detoxify the liver by producing antioxidants and detoxifying enzymes, thereby lowering reactive oxygen species (ROS) levels and other toxic metabolites to support liver function.

In conclusion, our findings fundamentally challenge the prevailing paradigm of tumor immunology by highlighting the primary role of anti-tumor immune responses in tissue homeostasis. Specifically, we demonstrate that alterations in hepatic homeostasis due to a WD during NAFLD not only drive carcinogenic events leading to HCC, but also promote host-protective immune responses through enhanced homeostatic pathways, rather than relying solely

on direct cytotoxicity against tumors. However, chronic exposure to carcinogenic WD can overwhelm these host-protective immune mechanisms, undermining the prevention of HCC. Crucially, the results reveal that dietary correction effectively alleviates this persistent carcinogenic pressure, enabling homeostatic immune responses to prevent HCC development. Consequently, effective immunotherapy for NAFLD and HCC should prioritize the promotion of immune responses that operate through tissue homeostasis, alongside measures to control carcinogenic pressures, rather than focusing solely on enhancing cytotoxic immune responses. This paradigm shift in our understanding of immune function has the potential to significantly refine therapeutic strategies, improving outcomes for patients with these conditions and paving the way for innovative treatment approaches that leverage the body's intrinsic ability to maintain tissue health and integrity.

References

1. Tacke F. Targeting hepatic macrophages to treat liver diseases. J Hepatol. Netherlands; 2017;66:1300–12.
2. Robinson MW, Harmon C, O'Farrelly C. Liver immunology and its role in inflammation and homeostasis. Cell Mol Immunol. China; 2016;13:267–76.
3. Nakashima H, Inui T, Habu Y, Kinoshita M, Nagao S, Kawaguchi A, et al. Activation of mouse natural killer T cells accelerates liver regeneration after partial hepatectomy. Gastroenterology. United States; 2006;131:1573–83.
4. Rao R, Graffeo CS, Gulati R, Jamal M, Narayan S, Zambirinis CP, et al. Interleukin 17-producing γδT cells promote hepatic regeneration in mice. Gastroenterology. United States; 2014;147:473-84.e2.
5. Anders RA, Subudhi SK, Wang J, Pfeffer K, Fu Y-X. Contribution of the lymphotoxin beta receptor to liver regeneration. J Immunol. United States; 2005;175:1295–300.
6. Kelly A, Fahey R, Fletcher JM, Keogh C, Carroll AG, Siddachari R, et al. $CD141^{+}$ myeloid dendritic cells are enriched in healthy human liver. J Hepatol. Netherlands; 2014;60:135–42.
7. Yahoo N, Dudek M, Knolle P, Heikenwälder M. Role of immune responses in the development of NAFLD-associated liver cancer and prospects for therapeutic modulation. J Hepatol. Netherlands; 2023;79:538–51.
8. Llovet JM, Willoughby CE, Singal AG, Greten TF, Heikenwälder M, El-Serag HB, et al. Nonalcoholic steatohepatitis-related hepatocellular carcinoma: pathogenesis and treatment. Nat Rev Gastroenterol Hepatol. England; 2023;20:487–503.

9. Koelsch N, Mirshahi F, Aqbi HF, Saneshaw M, Idowu MO, Olex AL, et al. The crosstalking immune cells network creates a collective function beyond the function of each cellular constituent during the progression of hepatocellular carcinoma. Sci Rep. England; 2023;13:12630.
10. Mirshahi F, Aqbi HF, Isbell M, Manjili SH, Guo C, Saneshaw M, et al. Distinct hepatic immunological patterns are associated with the progression or inhibition of hepatocellular carcinoma. Cell Rep. 2022;38:110454.
11. Parker TM, Gupta K, Palma AM, Yekelchyk M, Fisher PB, Grossman SR, et al. Cell competition in intratumoral and tumor microenvironment interactions. EMBO J. England; 2021;40:e107271.
12. Madan E, Pelham CJ, Nagane M, Parker TM, Canas-Marques R, Fazio K, et al. Flower isoforms promote competitive growth in cancer. Nature. England; 2019;572:260–4.
13. Asgharpour A, Cazanave SC, Pacana T, Seneshaw M, Vincent R, Banini BA, et al. A diet-induced animal model of non-alcoholic fatty liver disease and hepatocellular cancer. J Hepatol. 2016;65:579–88.
14. Idowu MO, Kmieciak M, Dumur C, Burton RS, Grimes MM, Powers CN, et al. CD44(+)/CD24(-/low) cancer stem/progenitor cells are more abundant in triple-negative invasive breast carcinoma phenotype and are associated with poor outcome. Hum Pathol. 2012;43:364–73.
15. Hao Y, Hao S, Andersen-Nissen E, Mauck WM 3rd, Zheng S, Butler A, et al. Integrated analysis of multimodal single-cell data. Cell. 2021;184:3573-3587.e29.
16. Hu C, Li T, Xu Y, Zhang X, Li F, Bai J, et al. CellMarker 2.0: an updated database of manually curated cell markers in human/mouse and web tools based on scRNA-seq data. Nucleic Acids Res. England; 2023;51:D870–6.
17. Guo H, Li J. scSorter: assigning cells to known cell types according to marker genes. Genome Biol. England; 2021;22:69.
18. Barrett T, Wilhite SE, Ledoux P, Evangelista C, Kim IF, Tomashevsky M, et al. NCBI GEO: archive for functional genomics data sets--update. Nucleic Acids Res. England; 2013;41:D991-5.
19. Guo M, Zhang H, Zheng J, Liu Y. Glypican-3: A New Target for Diagnosis and Treatment of Hepatocellular Carcinoma. J Cancer. Australia; 2020;11:2008–21.
20. Teeli AS, Łuczyńska K, Haque E, Gayas MA, Winiarczyk D, Taniguchi H. Disruption of Tumor Suppressors HNF4α/HNF1α Causes Tumorigenesis in Liver. Cancers (Basel). Switzerland; 2021;13.
21. Aqbi HF, Coleman C, Zarei M, Manjili SH, Graham L, Koblinski J, et al. Local and distant tumor dormancy during early stage breast cancer are associated with the predominance of infiltrating T effector subsets. Breast Cancer Res. England, England; 2020;22:116.
22. Payne KK, Keim RC, Graham L, Idowu MO, Wan W, Wang X-Y, et al. Tumor-reactive immune cells protect against metastatic tumor and induce immunoediting of indolent but not quiescent tumor cells. J Leukoc Biol. 2016;100.
23. Tkachenko E, Rhodes JM, Simons M. Syndecans: new kids on the signaling block. Circ Res. United States; 2005;96:488–500.
24. Clemmons DR. Role of insulin-like growth factor iin maintaining normal glucose homeostasis. Horm Res. Switzerland; 2004;62 Suppl 1:77–82.

25. Huang C-T, Chang M-C, Chen Y-L, Chen T-C, Chen C-A, Cheng W-F. Insulin-like growth factors inhibit dendritic cell-mediated anti-tumor immunity through regulating ERK1/2 phosphorylation and p38 dephosphorylation. Cancer Lett. Ireland; 2015;359:117–26.
26. Hu H, Cheng X, Li F, Guan Z, Xu J, Wu D, et al. Defective efferocytosis by aged macrophages promotes STING signaling mediated inflammatory liver injury. Cell death Discov. United States; 2023;9:236.
27. Grabiec AM, Goenka A, Fife ME, Fujimori T, Hussell T. Axl and MerTK receptor tyrosine kinases maintain human macrophage efferocytic capacity in the presence of viral triggers. Eur J Immunol. Germany; 2018;48:855–60.
28. Lhuillier C, Barjon C, Niki T, Gelin A, Praz F, Morales O, et al. Impact of Exogenous Galectin-9 on Human T Cells: CONTRIBUTION OF THE T CELL RECEPTOR COMPLEX TO ANTIGEN-INDEPENDENT ACTIVATION BUT NOT TO APOPTOSIS INDUCTION. J Biol Chem. United States; 2015;290:16797–811.
29. Wu C, Thalhamer T, Franca RF, Xiao S, Wang C, Hotta C, et al. Galectin-9-CD44 interaction enhances stability and function of adaptive regulatory T cells. Immunity. United States; 2014;41:270–82.
30. Chakraborty A, Staudinger C, King SL, Erickson FC, Lau LS, Bernasconi A, et al. Galectin-9 bridges human B cells to vascular endothelium while programming regulatory pathways. J Autoimmun. England; 2021;117:102575.
31. Bustelo XR. Vav family exchange factors: an integrated regulatory and functional view. Small GTPases. United States; 2014;5:9.
32. Dunn SE, Ousman SS, Sobel RA, Zuniga L, Baranzini SE, Youssef S, et al. Peroxisome proliferator-activated receptor (PPAR)alpha expression in T cells mediates gender differences in development of T cell-mediated autoimmunity. J Exp Med. United States; 2007;204:321–30.
33. Zhang MA, Rego D, Moshkova M, Kebir H, Chruscinski A, Nguyen H, et al. Peroxisome proliferator-activated receptor (PPAR)α and -γ regulate IFNγ and IL-17A production by human T cells in a sex-specific way. Proc Natl Acad Sci U S A. United States; 2012;109:9505–10.
34. Tumanov A V, Koroleva EP, Christiansen PA, Khan MA, Ruddy MJ, Burnette B, et al. T cell-derived lymphotoxin regulates liver regeneration. Gastroenterology. United States; 2009;136:694-704.e4.
35. Cuño-Gómiz C, de Gregorio E, Tutusaus A, Rider P, Andrés-Sánchez N, Colell A, et al. Sex-based differences in natural killer T cell-mediated protection against diet-induced steatohepatitis in Balb/c mice. Biol Sex Differ. England; 2023;14:85.
36. Zheng S, Yang W, Yao D, Tang S, Hou J, Chang X. A comparative study on roles of natural killer T cells in two diet-induced non-alcoholic steatohepatitis-related fibrosis in mice. Ann Med. England; 2022;54:2233–45.
37. Sutti S, Albano E. Adaptive immunity: an emerging player in the progression of NAFLD. Nat Rev Gastroenterol Hepatol. 2020;17:81–92.
38. Zhu H, Zhang Q, Chen G. CXCR6 deficiency ameliorates ischemia-reperfusion injury by reducing the recruitment and cytokine production of hepatic NKT cells in a mouse model of non-alcoholic fatty liver disease. Int Immunopharmacol. Netherlands; 2019;72:224–34.
39. Li X, Li R, Miao X, Zhou X, Wu B, Cao J, et al. Integrated Single Cell Analysis Reveals An

Atlas of Tumor Associated Macrophages in Hepatocellular Carcinoma. Inflammation. United States; 2024;
40. Sung PS, Park DJ, Roh PR, Mun K Do, Cho SW, Lee GW, et al. Intrahepatic inflammatory IgA(+)PD-L1(high) monocytes in hepatocellular carcinoma development and immunotherapy. J Immunother cancer. England; 2022;10.
41. Lurje I, Hammerich L, Tacke F. Dendritic Cell and T Cell Crosstalk in Liver Fibrogenesis and Hepatocarcinogenesis: Implications for Prevention and Therapy of Liver Cancer. Int J Mol Sci. Switzerland; 2020;21.
42. Ngo HV, Thanh Le TT, Vu HN, Hoang H, Ikenaga H, Sato-Matsubara M, et al. Poorly Differentiated Hepatocellular Carcinoma Cells Avoid Apoptosis by Interacting with T Cells via CD40-CD40L Linkage. Am J Pathol. United States; 2024;
43. Isbell M, Mirshahi F, Aqbi HF, Guo C, Saneshaw M, Koelsch N, et al. Restoration of CD4(+) T Cells during NAFLD without Modulation of the Hepatic Immunological Pattern Is Not Sufficient to Prevent HCC. Cancers (Basel). Switzerland; 2022;14.
44. Ilangumaran S, Borisch B, Hoessli DC. Signal transduction via CD44: role of plasma membrane microdomains. Leuk Lymphoma. United States; 1999;35:455–69.
45. Oh SK, Kim D, Kim K, Boo K, Yu YS, Kim IS, et al. RORα is crucial for attenuated inflammatory response to maintain intestinal homeostasis. Proc Natl Acad Sci U S A. United States; 2019;116:21140–9.
46. Han S, Li Z, Han F, Jia Y, Qi L, Wu G, et al. ROR alpha protects against LPS-induced inflammation by down-regulating SIRT1/NF-kappa B pathway. Arch Biochem Biophys. United States; 2019;668:1–8.
47. Kim K, Boo K, Yu YS, Oh SK, Kim H, Jeon Y, et al. RORα controls hepatic lipid homeostasis via negative regulation of PPARγ transcriptional network. Nat Commun. England; 2017;8:162.
48. Hu Q, Ye J, Zhu M-L, Jin Y, Yang X, Wu M. Dietary fructose promotes liver carcinogenesis by inducing the malignant transformation of hepatic progenitor cells. J Funct Foods [Internet]. 2021;82:104489. Available from: https://www.sciencedirect.com/science/article/pii/S1756464621001389
49. Manjili MH. The Adaptation Model of Immunity: Signal IV Matters Most in Determining the Functional Outcomes of Immune Responses. J Immunol. United States; 2023;210:521–30.
50. Van Der Byl W, Nüssing S, Peters TJ, Ahn A, Li H, Ledergor G, et al. The CD8(+) T cell tolerance checkpoint triggers a distinct differentiation state defined by protein translation defects. Immunity. United States; 2024;
51. Li T, Lin X, Shen B, Zhang W, Liu Y, Liu H, et al. Akkermansia muciniphila suppressing nonalcoholic steatohepatitis associated tumorigenesis through CXCR6(+) natural killer T cells. Front Immunol. Switzerland; 2022;13:1047570.
52. Sookoian S, Pirola CJ. Resmetirom for treatment of MASH. Cell. United States; 2024;187:2897-2897.e1.

Authors' Disclosures

A.J.S. and F.M. hold a patent on the DIAMOND mouse model, PCT/US2016/056506. All other authors do not have any competing interest.

Authors' Contributions

Conceptualization, M.H.M.; investigation, N.K., F.M., H.F.A., M.S., M.O.I.; writing first draft: N.K., M.H.M.; all authors edited the manuscript and approved the final submission; supervision: F.M., A.L.O., A.J.S, and M.H.M.; funding acquisition, M.H.M. and A.J.S. All authors reviewed the manuscript.

Acknowledgment

This work is supported by funding from NIH R01DK105961, Massey Comprehensive Cancer Center Muti-Investigator Award, grant number 2017-MIP-2, and the Office of the Assistant Secretary of Defense for Health Affairs through the Breast Cancer Research Program under Award No. W81XWH2210793. Opinions, interpretations, conclusions, and recommendations are those of the authors and are not necessarily endorsed by the U.S. Department of Defense. This work was also supported, in part, by CTSA award No. UL1TR002649 from the National Center for Advancing Translational Sciences, and from the VCU Cancer Mouse Models Core Shared Resource (CMMC) supported, in part, by funding from the NIH-NCI Cancer Center Support Grant P30 CA 016059.

Figure legends

Figure 1: Carcinogenic events take place prior to HCC and remain dormant during recovery from HCC. A) Representative liver images and histological Hematoxylin and Eosin (H&E) staining. B) UMAP of hepatic nonimmune cells (upper) and quantified nonimmune cell

proportions (lower). C) Violin Plots showing log-transformed average transcript expression of marker genes in cancer cell and hepatocyte populations such as Hnf4α, Rb1, Afp, and Gpc3. D) Violin Plot showing log-transformed average transcript expression in the Gpc3-filtered fraction of hepatocyte and cancer cells for each group. E) Quantification of the average transcript expression level of Hnf4α+ cells in the cancer cell population in each group. F) DotPlots showing the average expression level and percentage of cells expressing Mki67 (Ki67) (upper) in cancer cell (left) and hepatocyte (right) populations for the CD, WD.nf and RD.n groups, along with the average transcript expression in both cell populations after filtering for cells expressing Ki67 > 0 (lower).

Figure 2: Hepatic cells induce macrophage and monocyte-dominated immune responses through integrins for liver tissue integrity and homeostasis. A) Immune cell proportions quantified and normalized to 100% in the CD group. B) CellChat analysis heatmap showing results from 80% threshold analysis for Ligand (L) and Receptor (R) interactions in the CD group and representative chord diagram showing signaling directionality in the PARs pathway and the L-R contributions. C) CellChat analysis heatmap portraying results from 50% threshold analysis for L-R interactions in the CD group (upper), and representative chord diagrams showing signaling directionality in the IGF, FN1, GAS, and PARs dominant pathways and their L-R contributions (lower). D) CellChat analysis heatmap portraying results from 25% threshold analysis of L-R interactions in the CD group (upper), and the representative subdominant signaling chord diagrams detected for IGF, Galectin, Spp1, FN1, Laminin, Collagen, DHEAS, VTN, GAS, PARs, DHEA, and Cholesterol pathways and their L-R contributions (lower). E) DotPlots showing the percent expression and log-normalized average transcript expression of transcription factors involved in activation of T cells (left), NKT cells (middle left), NK cells

(middle), Macrophages (middle right), and Monocytes (right). Green text in L-R contributions denotes the cell type expressing receptors and Itga4+Itgb1 denotes VLA-4.

Figure 3: The number and strength of ligand-receptor interactions rather than cell type frequency determine the progression or inhibition of HCC. A) Comparative 50% threshold CellChat analysis quantifying the number of inferred interactions and overall interaction strength in each group. B) Cell-specific frequency (left panels) and comparative analysis in each group (right panels) showing overall incoming and outgoing interaction strength values for each cell type to evaluate major contributors to signaling networks.

Figure 4: HSCs, cancer cells and NKT cells dominate cellular interaction networks with NKT cells orchestrating the hepatic immune responses mainly through homeostatic pathways during WD-induced NAFLD progression: A) Immune and nonimmune cell proportions quantified and normalized to 100% in the WD.nf group. B) CellChat analysis heatmap from 80% threshold results (upper) and representative chord diagrams showing signaling directionality in Cholesterol, PARs, Galectin, and FN1 pathways and their L-R contributions (lower). C) DotPlot showing the percent expression and log-normalized average transcript expression of Cd1d1 in structural cells in the WD.nf group. D) CellChat heatmap analysis of 50% cell-cell interactions portraying all detected L-R signaling pathways (upper), and representative chord diagrams of signaling directionality in Cholesterol, PARs, Galectin, and FN1 pathways and their L-R contributions (lower). E) Quantification of cell-specific incoming and outgoing interaction strength in 50% CellChat analyses for nonimmune (upper panel) and immune cells (lower panel) in the CD and WD.nf groups. F) The differential number of signaling events sent (upper row) and received (lower row) detected in HSCs, cancer cells and NKT cells encompassing 50% of cell-cell interactions during NAFLD (WD.nf) compared to the CD group.

G) Signaling changes in 50% of cell-cell interactions in the WD.nf group compared to the CD group for HSCs, cancer and NKT cells. HSC, hepatic stellate cell; LSEC, liver sinusoidal endothelial cell; Fibro, fibroblasts; Hep, hepatocytes; Endo, endothelial cells; Cholangio, cholangiocytes; Myofibro, myofibroblasts; Neutro, neutrophils; Mac, macrophage; Mono, monocytes. Green text in L-R contributions denotes the cell type expressing receptors and Itga4+Itgb1 denotes VLA-4.

Figure 5: The hepatic cellular interactions dominated by cancer cells, hepatocytes, myofibroblasts and fibroblasts associated with NKT cell- and monocyte-dominated immune responses during HCC on a WD. A) Immune and nonimmune cell proportions quantified and normalized to 100% in the WD.t group. B) 80% CellChat analysis heatmap showing all L-R interactions in the WD.t group (upper), and representative chord diagrams showing signaling directionality in PARs, FN1, DHEAS, 27HC, and FGF pathways and their L-R contributions (lower). C) 50% CellChat analysis heatmap portraying all detected L-R pathway interactions in the WD.t group (upper panel), quantified incoming and outgoing interaction strength in nonimmune and immune cell populations (middle panel), and chord diagrams of signaling directionality in PARs, FN1, DHEAS, 27HC, and FGF pathways and their L-R contributions (lower panels). D) Dominant nonimmune cell differential number of interactions sent (left column), and received (right column) in cancer, hepatocytes, myofibroblasts, and fibroblasts in WD.t compared to WD.nf in 50% analyses. E) Dominant immune cell differential number of interactions sent (left column) and received (right column) in NKT cells and monocytes in 50% analyses. F) The 50% threshold analysis of signaling changes in cancer, NKT, hepatocyte, myofibroblast, fibroblast, and monocyte cell populations in WD.t compared to WD.nf. Green text in L-R contributions denotes the cell type expressing receptors and

Itga4+Itgb1 denotes VLA-4.

Figure 6: Stromal cell-dominated hepatic interactions, associated with diminished immune cell engagement, promote HCC whereas myofibroblasts dominance along with monocyte-dominated immune responses, prevent HCC following dietary correction. A) Immune (right panel) and nonimmune (left panel) cell proportions quantified and normalized to 100% in the RD.t and RD.n groups. B) 80% CellChat analysis heatmap in the RD.t and RD.n groups (upper), and the representative chord diagram of PARs in the RD.t group and PARs, DHEAS, NRG, and PROS in the RD.n group signaling directionality and the L-R contributions (lower). C) 50% CellChat analysis quantified incoming and outgoing interaction strength for nonimmune and immune cell populations (upper panel), heatmap of detected L-R pathways (middle panel), and chord diagrams of signaling directionality for PARs, DHEAS, PROS, FN1, VTN, Cholesterol, and FGF pathways and their L-R contributions (lower panel) in the RD.t (left) and RD.n (right) groups. D) 50% analysis showing the differential number of interactions sent (upper row) and received (lower row) for cancer, stromal cells, myofibroblasts, fibroblasts, hepatocytes, and monocytes across multiple comparisons such as CDvRD.t (left column), CDvRD.n (middle column), and RD.tvRD.n (right column). Green text in L-R contributions denotes the cell type expressing receptors and Itga4+Itgb1 denotes VLA-4.

Figure 7: Stromal cell-dominated hepatic interactions, associated with diminished immune cell engagement, promote HCC whereas myofibroblasts dominance along with monocyte-dominated immune responses, prevent HCC following dietary correction. A) Signaling changes present in stromal, cancer, myofibroblasts, fibroblasts, hepatocyte, and monocyte populations in RD.t compared to CD (CD vs. RD.t; upper panel), RD.n compared to CD (CD vs. RD.n; middle panel), and in RD.n compared to RD.t (RD.t vs. RD.n; lower panel). B) Chord

diagrams depicting signaling directionality of pathways detected in 50% CellChat analyses for RD.t (upper row) and RD.n (lower row) groups.

Figure 1

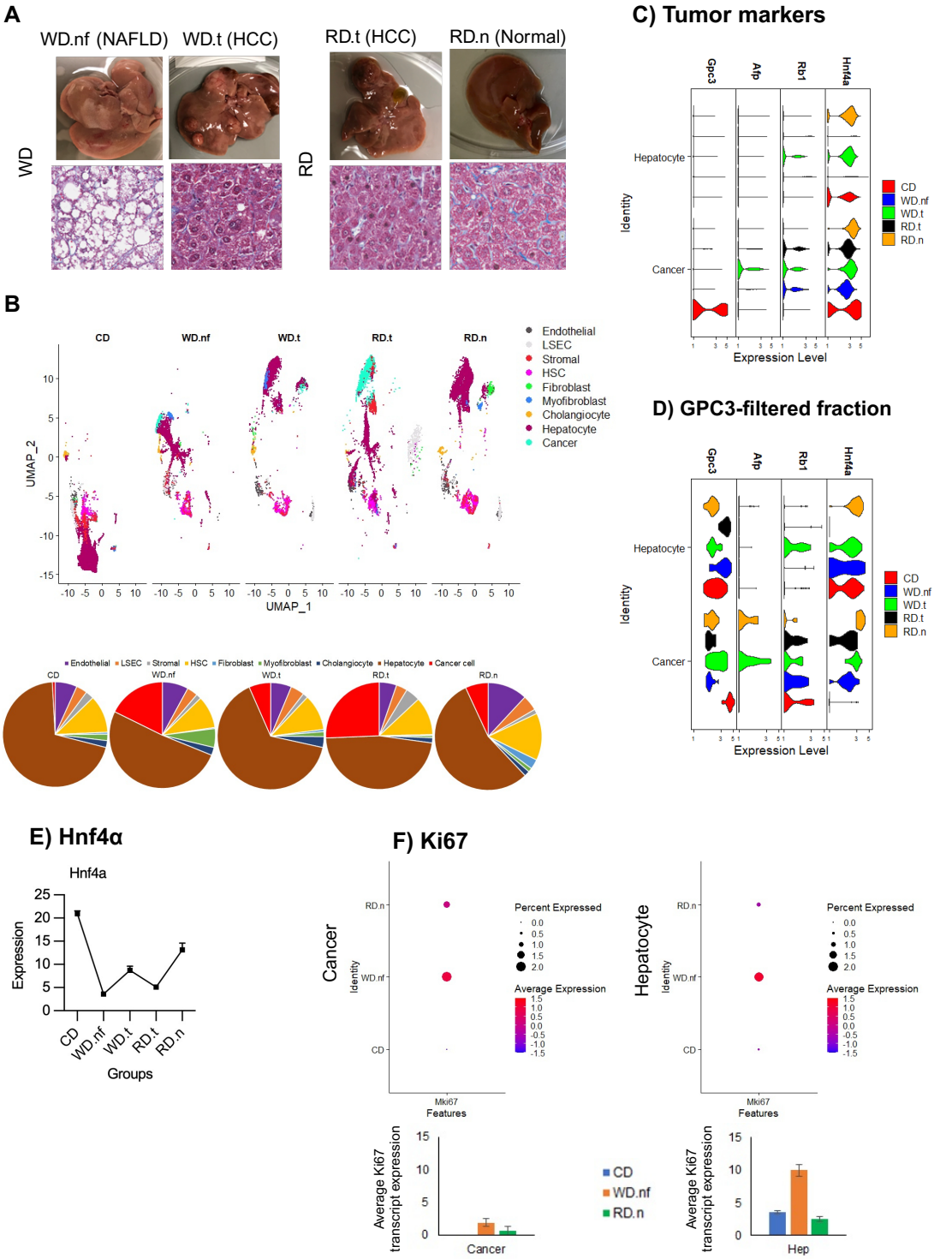
A
WD.nf (NAFLD)
WD.t (HCC)
RD.t (HCC)
RD.n (Normal)
WD
RD
B
CD
WD.nf
WD.t
RD.t
RD.n
UMAP_2
UMAP_1
Endothelial
LSEC
Stromal
HSC
Fibroblast
Myofibroblast
Cholangiocyte
Hepatocyte
Cancer
Endothelial LSEC Stromal HSC Fibroblast Myofibroblast Cholangiocyte Hepatocyte Cancer cell
C) Tumor markers
Gpc3
Afp
Rb1
Hnf4a
Hepatocyte
Cancer
Identity
Expression Level
CD
WD.nf
WD.t
RD.t
RD.n
D) GPC3-filtered fraction
E) Hnf4α
Hnf4a
Expression
Groups
F) Ki67
Cancer
Hepatocyte
Percent Expressed
Average Expression
Mki67
Features
Average Ki67 transcript expression
Hep

Figure 2

A) Cellular pattern

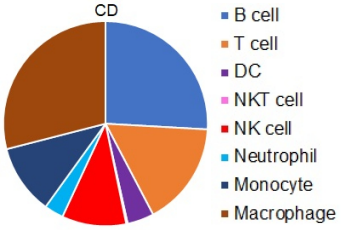

B) The 80% cell-cell interactions

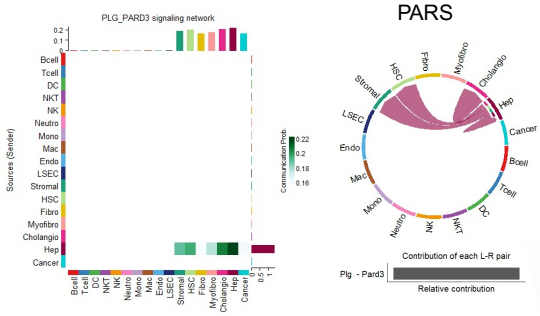

C) The 50% cell-cell interactions

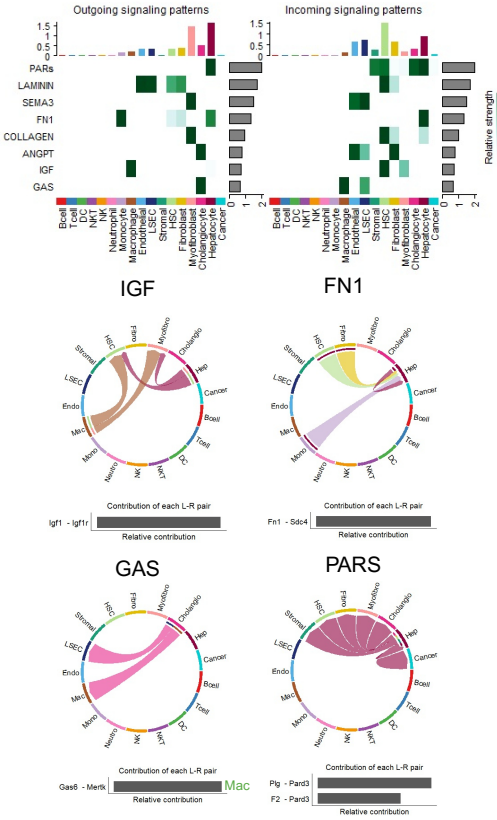

D) The 25% cell-cell interactions

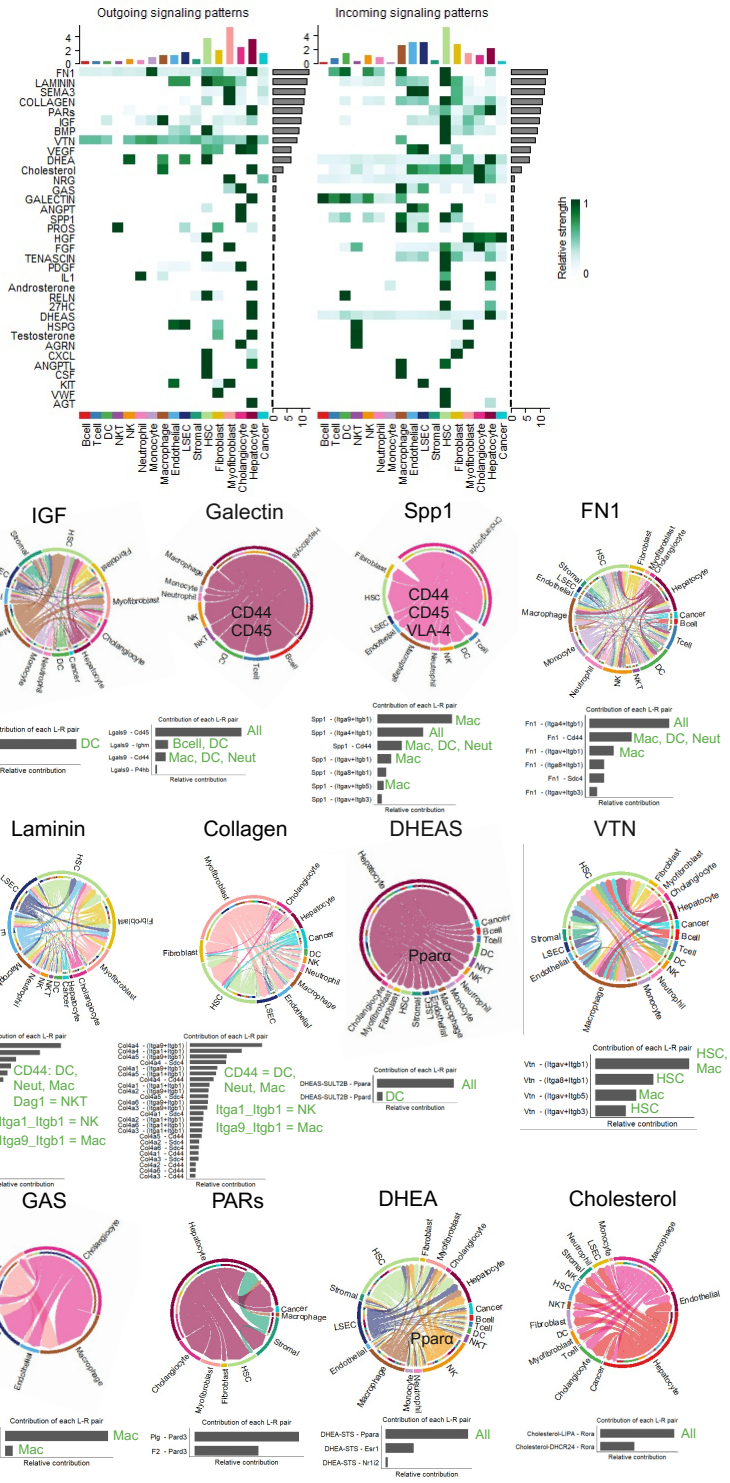

E) Transcription factor expression

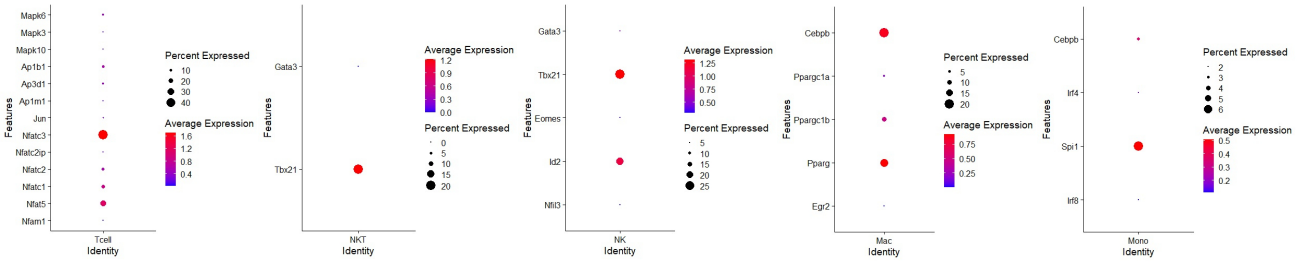

Figure 3

A) The quantified ligand-receptor interactions

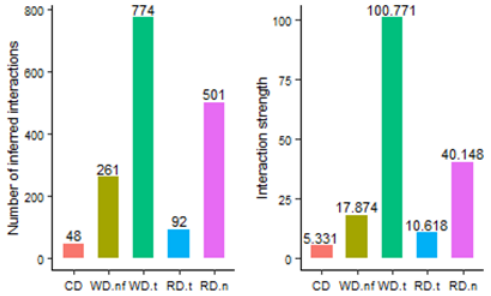

B) Cell-specific frequency & ligand-receptor interactions

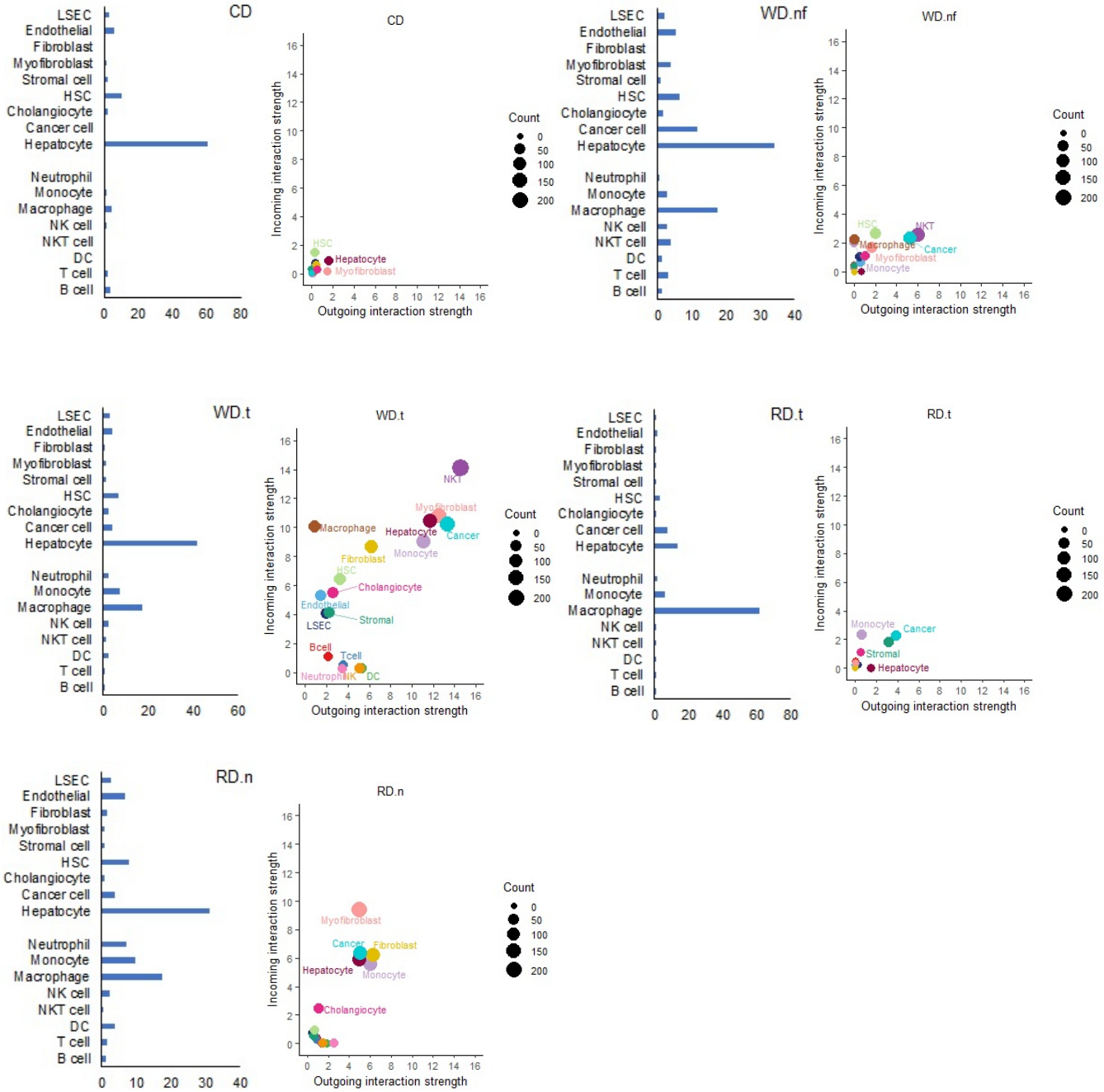

Figure 4

A) Cellular pattern

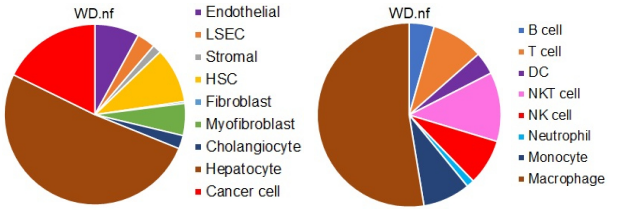

B) The 80% cell-cell interactions

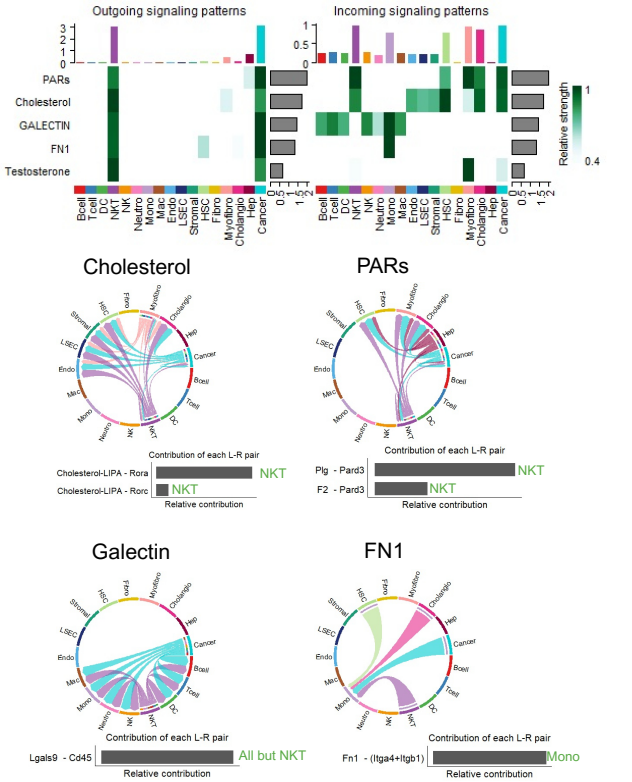

C) Cd1d1 Expression

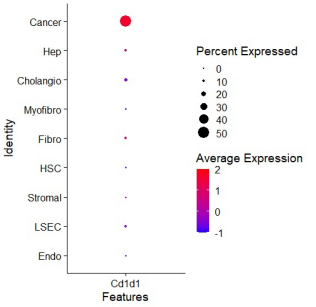

D) The 50% cell-cell interactions

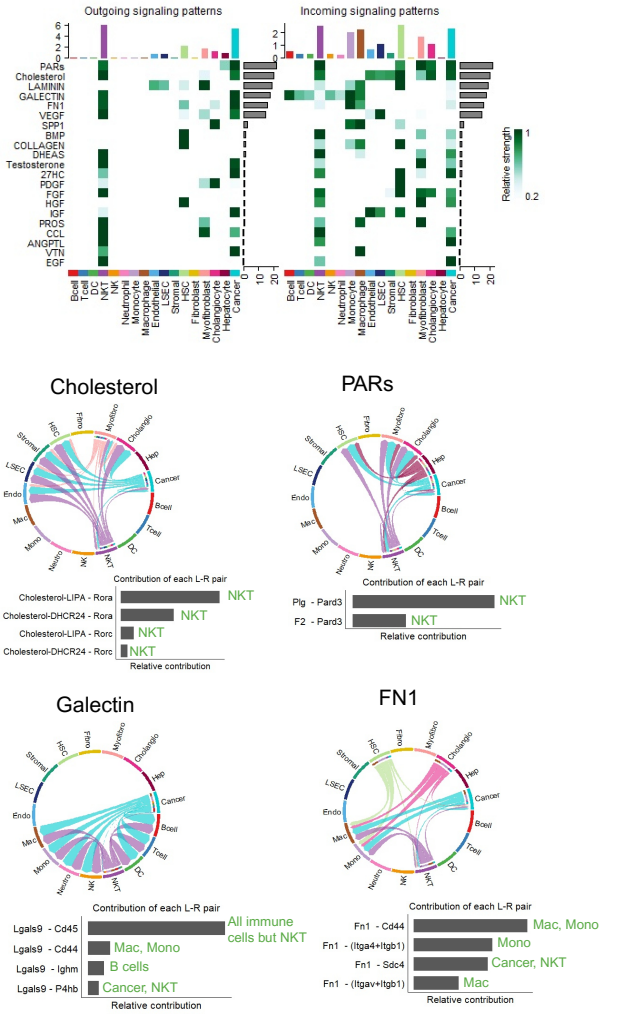

E) 50% Incoming-outgoing signals

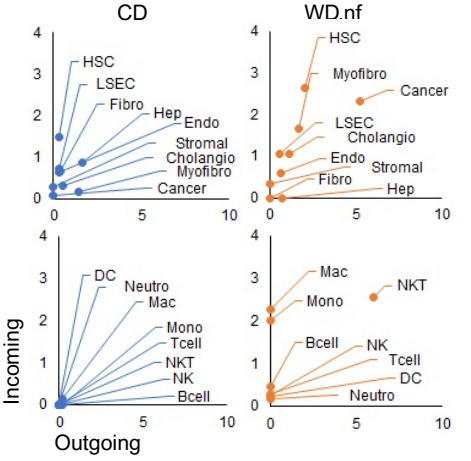

F) WD.nf vs. CD

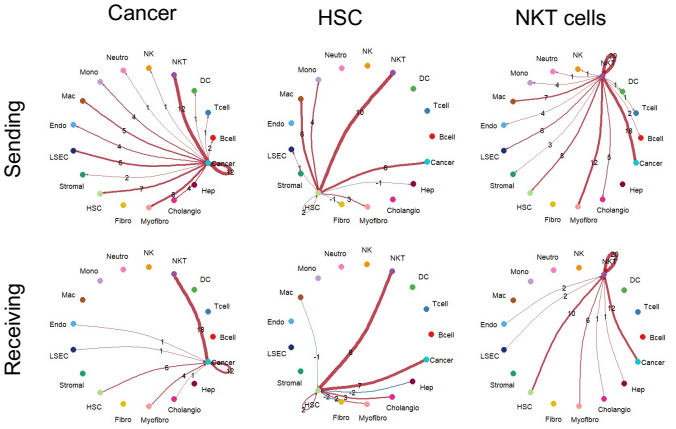

G) Hepatic homeostatic pathways

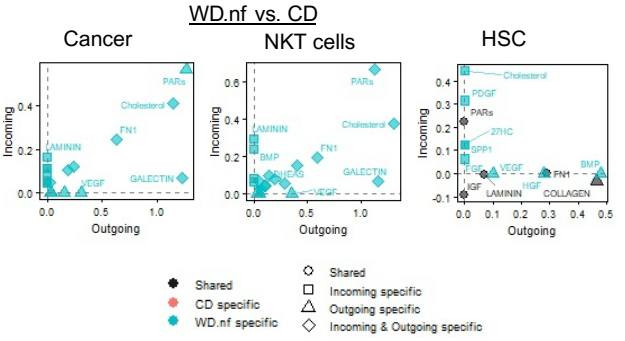

Figure 5

A) Cellular pattern during HCC

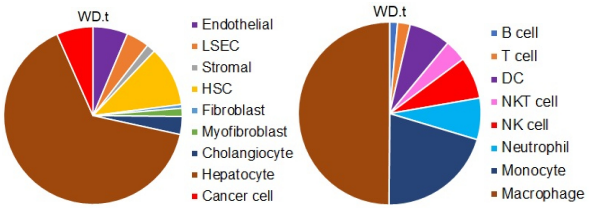

B) 80% Ligand-receptor interactions

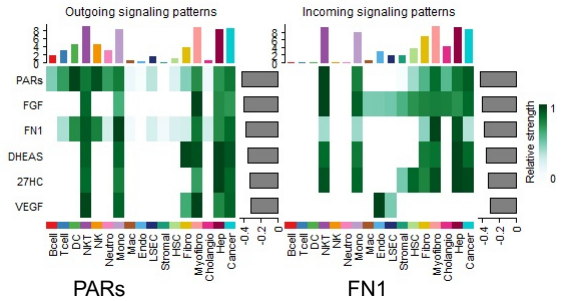

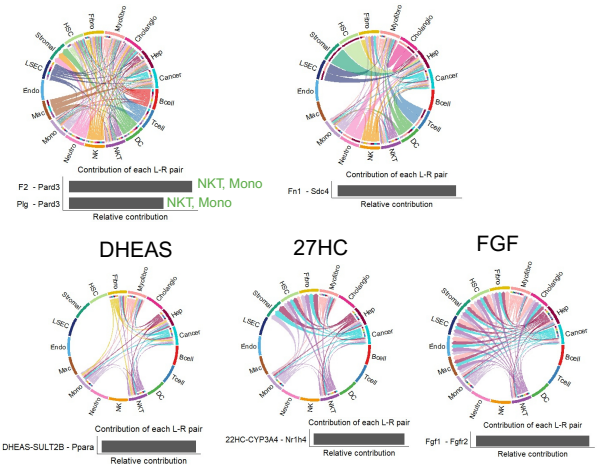

C) 50% Ligand-receptor interactions

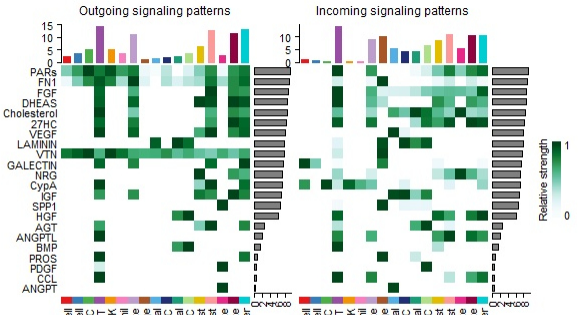

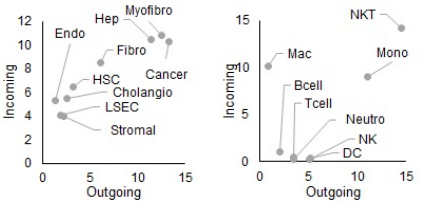

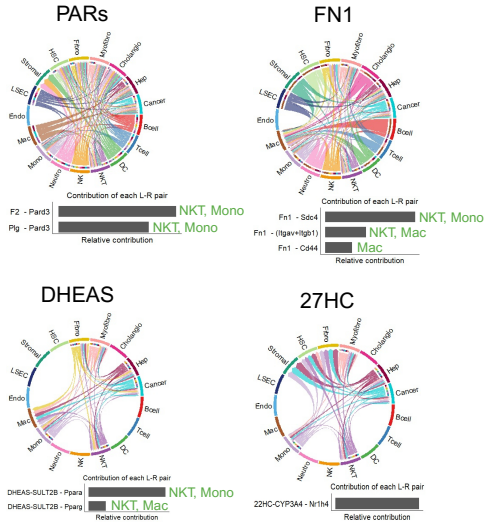

D) Nonimmune cells (WD.t vs. WD.nf)

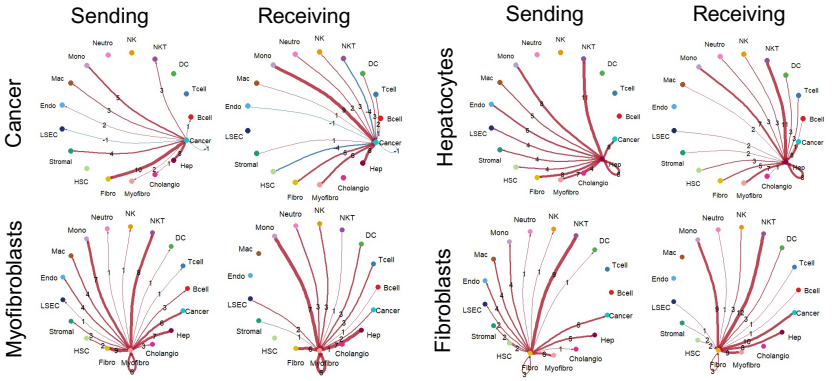

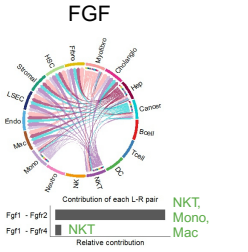

E) Immune cells (WD.t vs. WD.nf)

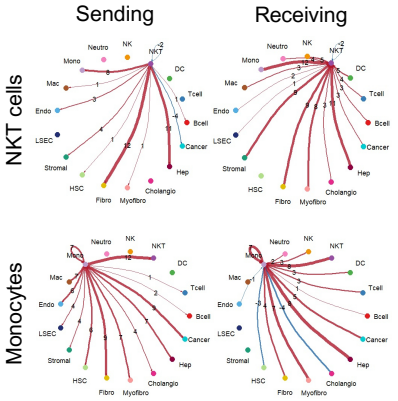

F) Signaling Pathways (WD.t vs. WD.nf)

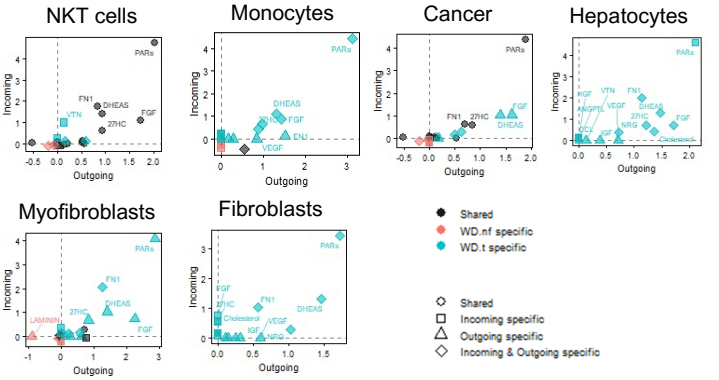

Figure 6

A) Cellular pattern

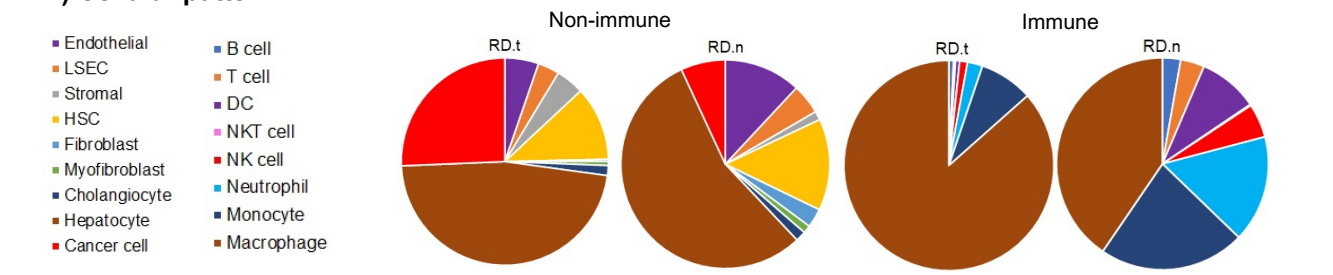

B) 80% Ligand-Receptor Interactions

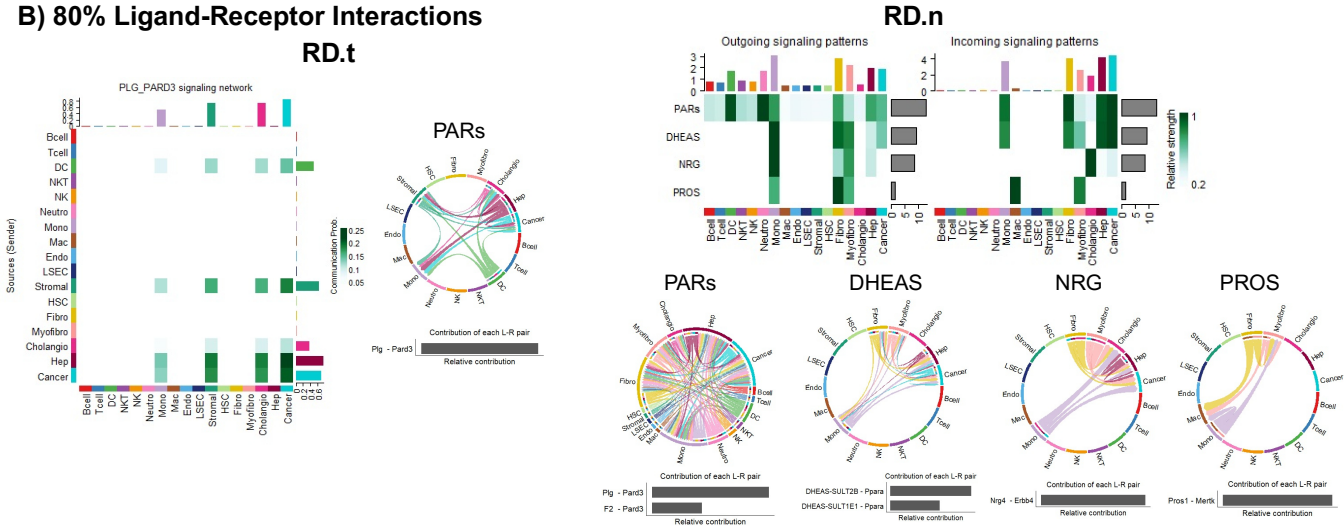

C) 50% Ligand-Receptor Interactions

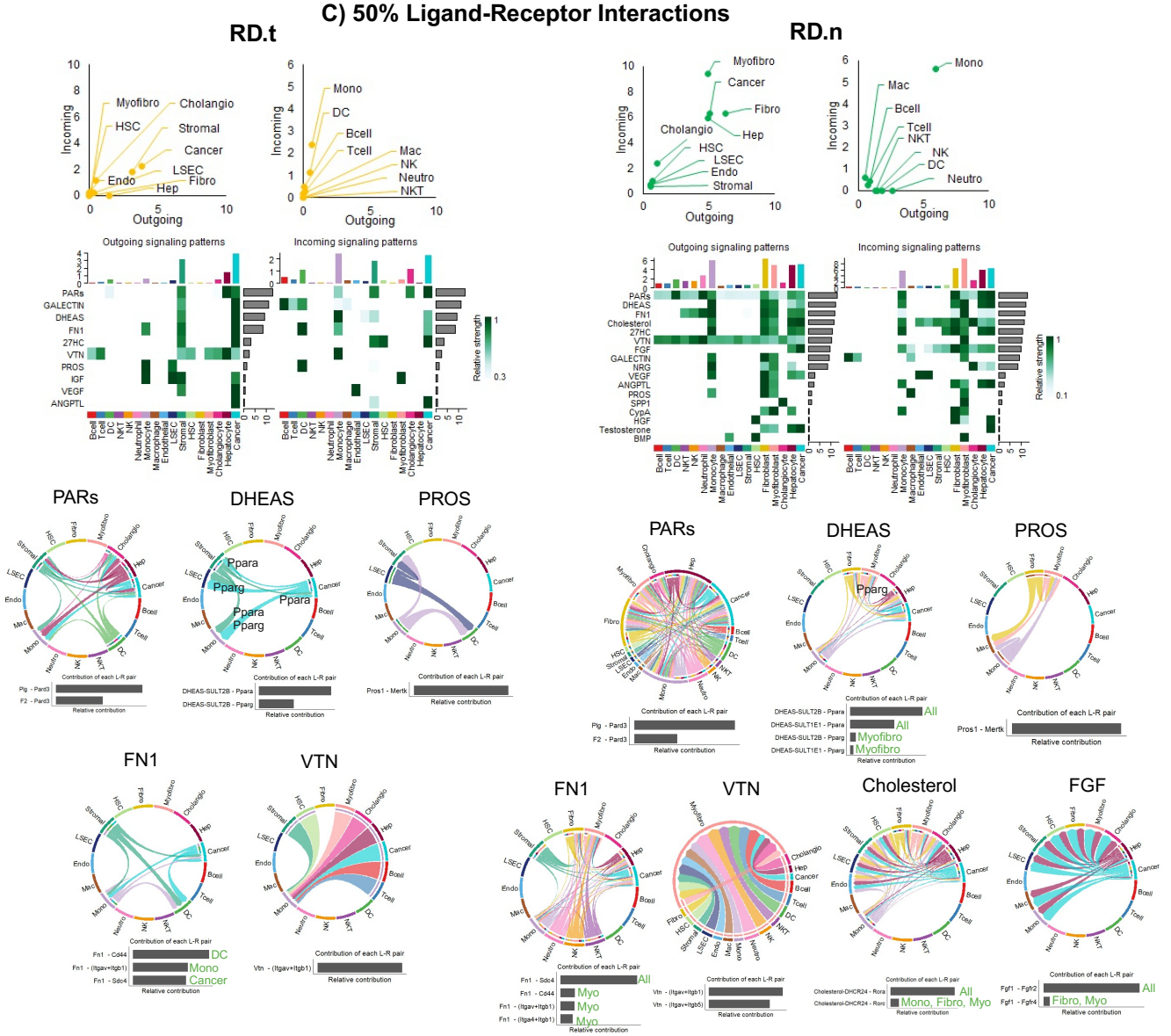

Figure 6

D) Signaling directionality

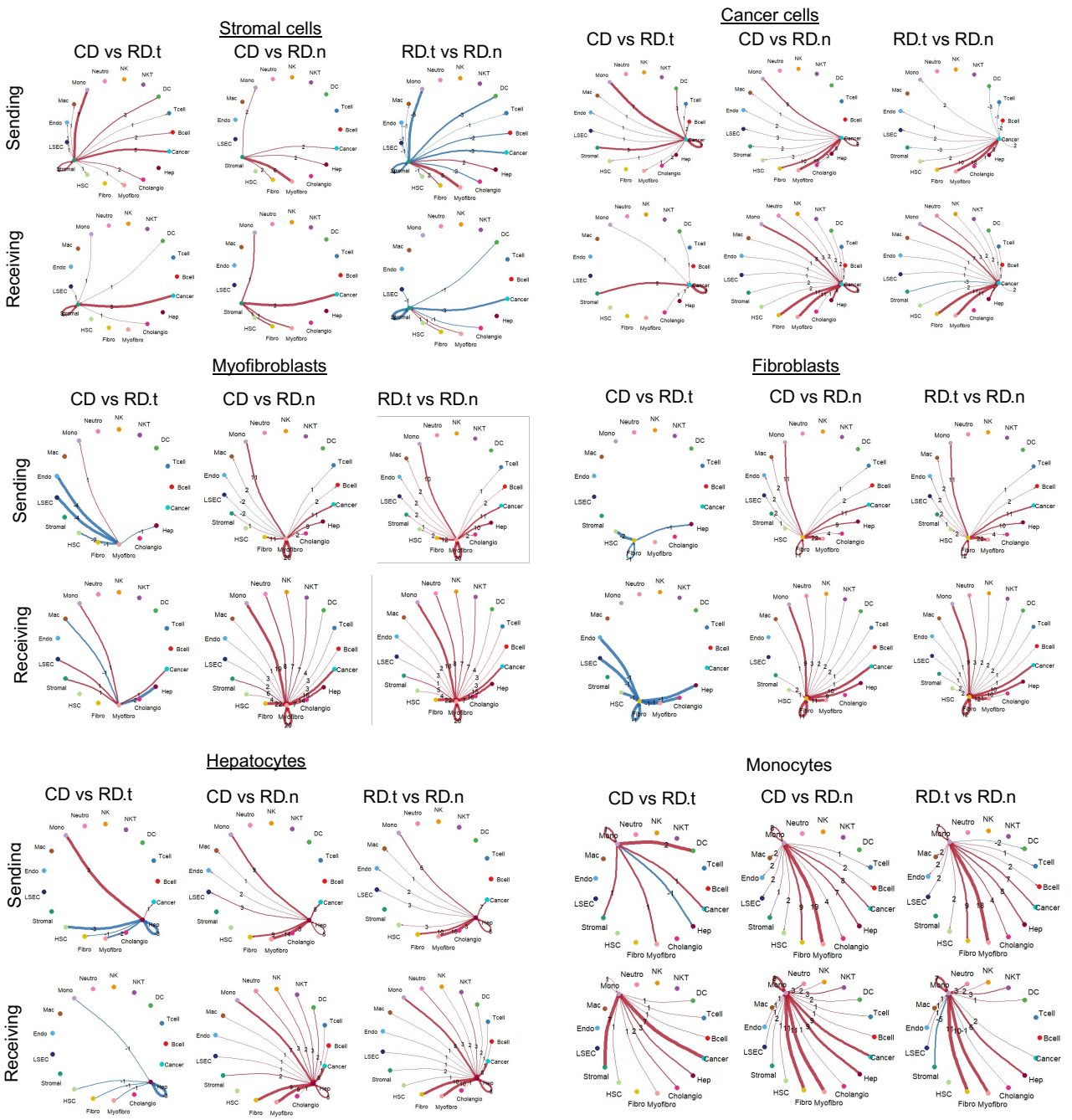

Figure 7

A) Signaling pathways

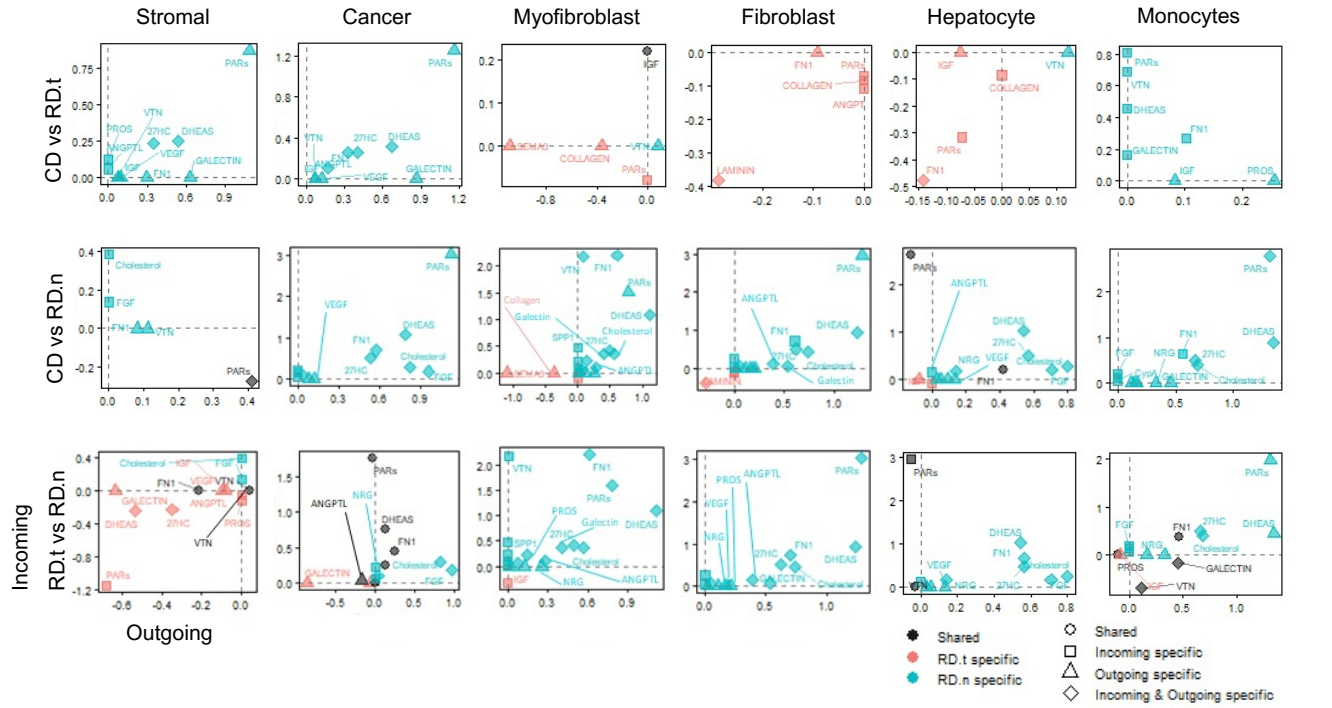
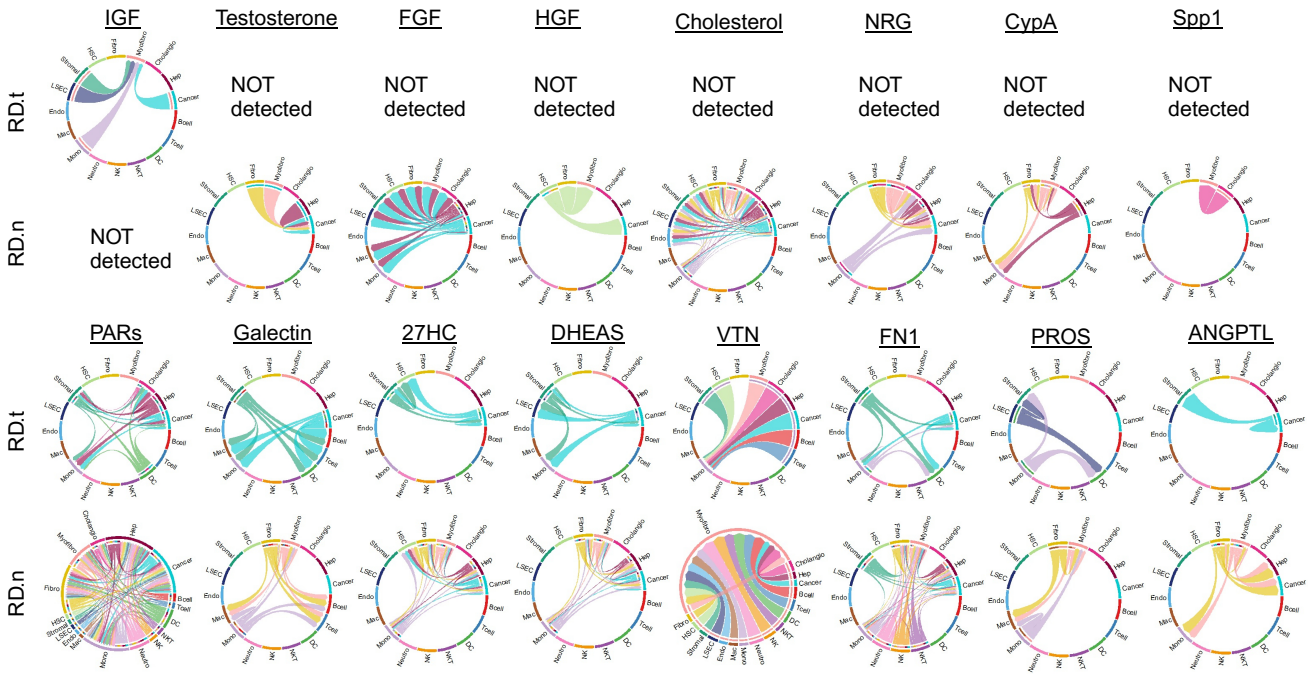
B) Signaling directionality